Remote Sensing of Environment 252 (2021) 112189

Contents lists available at ScienceDirect

Remote Sensing of Environment

journal homepage: www.elsevier.com/locate/rse

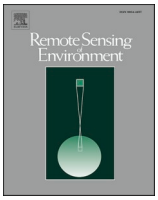

Interoperability of ECOSTRESS and Landsat for mapping evapotranspiration time series at sub-field scales

Martha C. Anderson [a,*], Yang Yang [a], Jie Xue [a], Kyle R. Knipper [a], Yun Yang [a,b], Feng Gao [a], Chris R. Hain [c], William P. Kustas [a], Kerry Cawse-Nicholson [d], Glynn Hulley [d], Joshua B. Fisher [d], Joseph G. Alfieri [a], Tilden P. Meyers [e], John Prueger [f], Dennis D. Baldocchi [g], Camilo Rey-Sanchez [g]

[a] USDA ARS, Hydrology and Remote Sensing Laboratory, Beltsville, MD, USA
[b] Earth System Science Interdisciplinary Center, University of Maryland, College Park, MD, USA
[c] NASA Marshall Space Flight Center, Earth Science Branch, Huntsville, AL, USA
[d] Jet Propulsion Laboratory, California Institute of Technology, Pasadena, CA, USA
[e] Atmospheric Turbulence and Diffusion Division, National Oceanic and Atmospheric Administration, Oak Ridge, TN, USA
[f] USDA ARS, National Laboratory for Agriculture and The Environment, Ames, IA, USA
[g] University of California – Berkeley, Berkeley, CA, USA

ARTICLE INFO

Keywords:
ECOSTRESS
Landsat
Evapotranspiration
Thermal infrared
Land-surface temperature
Surface energy balance
Water use

ABSTRACT

Land-surface temperature retrieved from thermal infrared (TIR) remote sensing has proven to be a valuable constraint in surface energy balance models for estimating evapotranspiration (ET). For optimal utility in agricultural water management applications, frequent thermal imaging (<4-day revisit) at sub-field (100 m or less) spatial resolution is desired. While, the current suite of Landsat satellites (7 and 8) provides the required spatial resolution, the 8-day combined revisit can be inadequate to capture rapid changes in surface moisture status or crop phenology, particularly in areas of persistent cloud cover. The new ECOsystem Spaceborne Thermal Radiometer Experiment on Space Station (*ECOSTRESS*) mission, with an average 4-day revisit interval and nominal 70-m resolution, provides a valuable research platform for augmenting Landsat TIR sampling and for investigating TIR-based ET mapping mission requirements more broadly. This study investigates the interoperability of Landsat and ECOSTRESS imaging for developing ET image timeseries with high spatial (30-m) and temporal (daily) resolution. A data fusion algorithm is used to fuse Landsat and ECOSTRESS ET retrievals at 30 m with daily 500-m retrievals using TIR data from the Moderate Resolution Imaging Spectroradiometer (MODIS) over target agricultural sites spanning the United States.The added value of the combined multi-source dataset is quantified in comparison with daily flux tower observations collected within these target domains. In addition, we investigate ET model performance as a function of ECOSTRESS view angle, overpass time, and time separation between TIR and Landsat visible to shortwave infrared (VSWIR) data acquisitions used to generate land-surface temperature, leaf area index, and albedo inputs to the surface energy balance model. The results demonstrate the value of the higher temporal sampling provided by ECOSTRESS, especially in areas that are frequently impacted by cloud cover. Limiting usage to ECOSTRESS scenes collected between 9:00 a.m. to 5:00 p.m. and nadir viewing angles <20° yielded daily (24-h) ET retrievals of comparable quality to the well-tested Landsat baseline. We also discuss challenges in using land-surface temperature from a thermal free-flyer system for ET retrieval, which may have ramifications for future TIR water-use mapping missions.

1. Introduction

Thermal infrared (TIR)-based surface energy balance (SEB) modeling has proven to be an effective tool for mapping consumptive water use in agricultural systems over a range in spatial scales – from sub-field to global coverage. Land-surface temperature (LST) maps retrieved from TIR remote sensing provide a valuable proxy measure of the surface moisture status, effectively constraining latent heat (energy flux) and

* Corresponding author at: 10300 Baltimore Ave, Beltsville, MD 20705, United States of America.
E-mail address: martha.anderson@usda.gov (M.C. Anderson).

https://doi.org/10.1016/j.rse.2020.112189
Received 6 July 2020; Received in revised form 8 October 2020; Accepted 9 November 2020
Available online 20 November 2020

evapotranspiration (ET; mass flux) estimates from SEB models at the image pixel scale (Kalma et al., 2008; Kustas and Anderson, 2009). In particular, Landsat thermal imaging has been broadly demonstrated as having operational utility for on-farm and regional water management and decision making (Anderson et al., 2012a). In combination with the visible to shortwave infrared (VSWIR) reflectance bands collected on the same platform, Landsat thermal data enable global sub-field scale ET mapping back to the launch of Landsat 4 in 1982. Landsat-scale daily ET information has been used to support a range in management activities, from irrigation scheduling (Knipper et al., 2019a) to water rights compliance monitoring (Allen et al., 2007) to water allocation and accounting (Cuenca et al., 2013; Karimi et al., 2013; Senay et al., 2016; Medellín-Azuara et al., 2018).

The effectiveness of SEB-based ET mapping tools is currently limited by the temporal revisit of medium resolution (defined here as ~100 m) TIR sensors like Landsat. The 8 to 16-day Landsat revisit frequency provided by 2 or 1 concurrent platforms, respectively, can miss changes in vegetation water use and stress that will impact monitoring and management goals, especially in areas impacted by frequent cloud cover (Anderson et al., 2012a; Senay et al., 2016; Alfieri et al., 2017a; Guillevic et al., 2019). The need for higher temporal sampling at medium resolution in contemporaneous VSWIR and TIR measurements is a prime factor in determining requirements for future sustainable land imaging missions (e.g., Landsat 10 and beyond) (Fisher et al., 2017; Wu et al., 2019). New Earth-observing platform architectures are being explored to address temporal sampling while reducing mission costs, including disaggregation of TIR and VSWIR instrumentation onto separate platforms. Given the value of Landsat-like TIR imaging to water resource management, it is important to understand the ramifications of thermal free-flyer (i.e., collecting TIR imagery only) strategies on ET retrieval accuracy and to quantify the value added by more frequent temporal revisit.

Another important consideration for future water-use mapping missions is optimal TIR sensor overpass time. At the 100-m scale, at present we are limited in broad-scale testing to typical Landsat overpass times, constrained to an equatorial crossing time of 10:00 a.m. ±15 m over much of the archive. However, simulations and field studies suggest that an early afternoon overpass would better capture stress conditions resulting in midday stomatal closure and reduced afternoon transpiration fluxes (Tuzet et al., 2003; Leuning et al., 2004). The Moderate Resolution Imaging Spectroradiometer (MODIS) on-board the Aqua platform collects routine 1-km nadir resolution TIR imagery at 1:30 p.m., but not at the field to sub-field scales where crop-specific stress variability is most suitably captured. The 375-m I5 thermal band from the Visible Infrared Imaging Radiometer Suite (VIIRS) on-board the Joint Polar Satellite System (JPSS) missions (1:30 p.m. overpass) gets closer to the goal; however, there are no current standard LST products produced from the VIIRS I5 band.

The ECOsystem Spaceborne Thermal Radiometer Experiment on Space Station (*ECOSTRESS*) mission provides a valuable research platform for investigating TIR-based ET mapping mission requirements more broadly (Fisher et al., 2017; Fisher et al., 2020). Launched to the International Space Station (ISS) in June of 2018, the TIR-only ECOSTRESS mission gives us the opportunity to study the value of enhanced temporal sampling in medium-resolution thermal imaging, the impacts of TIR/VSWIR separation, and alternate overpass times in the context of different ET modeling systems. The ISS orbit provides coverage between ±52° latitude with overpass at varying times of day, and sometimes multiple revisits per day depending on latitude and time of year. Over the continental USA (CONUS) this translates into an average revisit time of every four days, at different times of day. The original mission supported two ET mapping approaches for generation of Level 3 (L3) ET and Level 4 (L4) Evaporative Stress products: the PT-JPL method (Fisher et al., 2008), which uses TIR to constrain net radiation within a Priestley-Taylor (PT) based estimate of actual ET; and the Atmosphere-Land Exchange Inverse (ALEXI) disaggregation method (DisALEXI), which uses LST in a full energy balance model to downscale regional ALEXI ET flux fields (Norman et al., 2003; Anderson et al., 2004). Initial performance evaluation of PT-JPL ECOSTRESS products has been reported by Fisher et al. (2020).

Here we compare ECOSTRESS TIR-based ET retrievals from the DisALEXI SEB model with Landsat-based estimates over a set of agricultural sites spanning CONUS for 2018, the first calendar year of ECOSTRESS operation. DisALEXI applications with Landsat have been well-documented (e.g., Anderson et al., 2012b; Cammalleri et al., 2014a; Sun et al., 2017; Anderson et al., 2018; Yang et al., 2018; Yang et al., 2020), so the Landsat retrievals serve as a baseline for evaluating ECOSTRESS performance and the potential for interoperability of these two sources of medium-resolution thermal imaging toward improved daily ET estimation at sub-field scales. Landsat and ECOSTRESS retrievals are compared for consistency in spatial and temporal patterns, and to identify dependencies on sensor view angle, overpass time, and TIR-VSWIR separation interval. Landsat-only and Landsat + ECOSTRESS timeseries are further fused with daily 500-m estimates from MODIS to generate multi-source ET datacubes at 30-m spatial and daily temporal resolution. The value of the additional temporal sampling afforded by ECOSTRESS is quantified in comparison with daily and weekly ET observations from a suite of flux towers within the modeling domains. We also discuss challenges in using LST from a thermal free-flyer system for ET retrieval, which may have ramifications for future TIR water-use mapping missions.

2. Study domain

ET datacubes based on Landsat and Landsat+ECOSTRESS medium-resolution LST retrievals were constructed for 2018 over nine study sites across the United States (Fig. 1). These sites cover a range in climate and cloud cover conditions, with a focus on croplands – both rainfed and irrigated. Of these, the California domains provide a best-case scenario in terms of cloud cover where Landsat 7 and 8 alone are typically sufficient to reasonably capture seasonal ET dynamics, although this is not always the case in landcovers where conditions vary rapidly (e.g., alfalfa). Sites in the Midwest Corn Belt and in Maryland represent agricultural regions with higher cloud cover frequency where extra TIR temporal sampling can be very beneficial.

Each site contains one or more flux towers for model evaluation, most of which had processed datasets for 2018 available at the time of writing (Table 1). Many are part of the USDA Agricultural Research Service Long-Term Agroecosystem Research (LTAR) network, focused on providing high quality long-term datasets supporting research in agricultural sustainability (Kleinman et al., 2018). Each datacube was approximately 90 × 90 km in dimension, with 30 m pixels and daily timesteps covering the full year.

Three ET data fusion domains are maintained over a north-south gradient in California in support of the Grape Remote sensing Atmospheric Profile and Evapotranspiration eXperiment (GRAPEX) project (Kustas et al., 2018). These domains are focused on irrigated vineyards selected to represent a climatic gradient in wine production regions in California – from the southern Central Valley in Madera County (Ripperdan grape production area), to a centrally located site in Sacramento County (Sierra Loma), to a northern site in Sonoma County (Barrelli). The Sierra Loma domain also includes AmeriFlux towers with tower data availability in the California Delta region (Bouldin Island), situated in fields cultivated with irrigated corn and alfalfa in 2018. The overall region is characterized by a Mediterranean climate, with predominantly clear skies outside of the winter rainy season, but with a gradient in increasing aridity and temperature from north to south (Knipper et al., 2020). In combination, these sites provide a valuable high temporal density baseline of clear-sky Landsat ET retrievals for comparison with ECOSTRESS retrievals (Semmens et al., 2015; Knipper et al., 2019a, 2019b, 2020; Anderson et al., 2018, 2019).

Three sites across the Midwest represent a gradient in rainfall, cloud

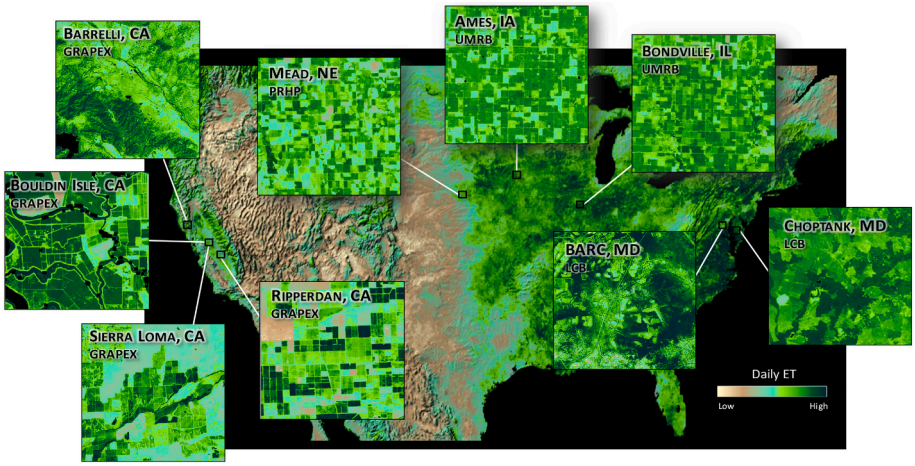

Fig. 1. Study domains included in the model intercomparisons. Background map shows ETd from ALEXI (4 km), while inset maps are 30-m resolution maps from DisALEXI over flux tower sites.

Table 1
Flux towers used in the analysis, listing surrounding landcover in 2018.

Site	State	Tower	Cover	Latitude	Longitude
Ripperdan	CA	RIP760	vineyard	36.8391	−120.2101
Sierra Loma	CA	SLM001	vineyard	38.2894	−121.1178
Sierra Loma	CA	SLM002	vineyard	38.2805	−121.1176
Bouldin Island	CA	US-Bi1	alfalfa	38.0991	−121.4993
Bouldin Island	CA	US-Bi2	corn	38.1090	−121.5350
Barrelli	CA	BAR012	vineyard	38.7514	−122.9747
Mead	NE	US-Ne1	corn	41.1650	−96.4766
Mead	NE	US-Ne2	soybean	41.1651	−96.4701
Mead	NE	US-Ne3	soybean	41.1798	−96.4399
Bondville	IL	US-Bo1	soybean	40.0519	−88.3731
BARC	MD	OPE3	soybean	39.0309	−76.8443
Choptank	MD	CHOP	soybean	39.0587	−75.8513

cover and irrigation practices within the U.S. Corn Belt. The Mead, NE and Ames, IA domains cover watersheds in the Platte River – High Plains (PRHP) and Upper Mississippi River Basin (UMRB) LTAR sites, while Bondville, IL lies within the Central Mississippi River Basin (CMRB) region. These sites are characterized predominantly by corn-soybean rotation cropping systems with a decrease in irrigation prevalence from west to east. DisALEXI performance for mapping ET and ET-based stress indicators in the Corn Belt has been assessed using Landsat (Cammalleri et al., 2014a; Yang et al., 2018).

Two additional domains in Maryland provide coverage over the ARS Lower Chesapeake Bay (LCB) LTAR site on the U.S. East Coast. The Optimizing Production Inputs for Economic and Environmental Enhancement (OPE3) long-term measurement site is located in the Beltsville Agricultural Research Center (BARC) domain (Gish et al., 2003; Alfieri et al., 2017b). This domain also includes the Washington D. C. and Baltimore metro areas, facilitating investigation of water use in urban landcovers. The Choptank domain covers the Choptank River watershed on Maryland's Eastern Shore, where ARS research focuses on impacts of agriculture on water quality in the Chesapeake Bay (McCarty et al., 2008). Both sites have been used for SEB and DisALEXI-Landsat evaluation (Houborg et al., 2011; Sun et al., 2017).

3. Materials and methods

3.1. ALEXI/DisALEXI energy balance model

The USDA-ARS ALEXI/DisALEXI algorithm is described in detail in the ECOSTRESS Level 3 Evapotranspiration (ALEXI-ET) Algorithm Theoretical Basis Document (ATBD) (Anderson, 2018) and references therein, and is summarized here.

ALEXI/DisALEXI is a multi-scale SEB modeling system designed to generate self-consistent flux assessments from field to regional/continental scales (Anderson et al., 2003). Both ALEXI and DisALEXI use the Two-Source Energy Balance (TSEB) land-surface representation to partition surface temperature fluxes between the canopy and the soil components of the model pixel (Norman et al., 1995; Kustas and Norman, 1999, 2000). LST is the primary remote sensing input to the TSEB, directly constraining estimates of sensible heat and net radiation, and indirectly latent heat by residual. The TSEB also uses satellite-derived estimates of leaf area index (LAI) to govern the soil/canopy partitioning and albedo to compute net radiation.

The regional Atmosphere-Land Exchange Inverse (ALEXI) model applies the TSEB to two morning measurements of LST, typically acquired at resolutions of several kilometers from geostationary satellites, and iteratively balances the time-integrated sensible heat flux within the surface-atmospheric boundary layer system (Anderson et al., 1997; Mecikalski et al., 1999; Anderson et al., 2007). In this study, estimates of morning latent heat flux have been upscaled to daily values as a scaled ratio of daily insolation (Cammalleri et al., 2014b), then converted to daily total ET (ETd; mm d^{-1}) using the latent heat of vaporization and the density of water.

ALEXI ET data are routinely produced at 4-km resolution over the U. S. using thermal imagery from the Geostationary Operational Environmental Satellites (GOES) (see background image in Fig. 1). For applications requiring finer scale (sub-km) ET information, these regional ALEXI ET maps can be spatially disaggregated using higher resolution LST information from polar orbiting systems (e.g., Landsat or MODIS), platforms such as the ISS (e.g., ECOSTRESS), or from aircraft using the DisALEXI algorithm (Norman et al., 2003; Anderson et al., 2004). In DisALEXI, the TSEB is implemented at the time of satellite overpass, daily ET is computed, and the upper boundary condition in air temperature is iteratively adjusted until the reaggregated fluxes match the ALEXI baseline ETd at the ALEXI pixel scale (Sun et al., 2017). In this way, evaporative flux matching across scales is enforced at the daily timescale, and LST data from thermal sensor overpasses at arbitrary time of day can in theory be accommodated. The ECOSTRESS orbit on the ISS facilitates testing of practical limits to useful thermal image acquisition time-of-day for ALEXI disaggregation.

3.2. ET datcube construction

To generate sub-field scale ET maps at daily timesteps, as required for many applications, periodic ET retrievals from Landsat-like sensors must be interpolated between overpass dates. This is often accomplished

using a scaling flux that can be derived from standard meteorological datasets, such as solar radiation, evaporative fraction, or reference ET (Ryu et al., 2012; Alfieri et al., 2017a). Alternatively, ET maps from thermal sensors with coarser resolution but more frequent overpass interval can be used as a scaling flux informing daily interpolation.

The ET datacube processing flow used in this study is diagrammed schematically in Fig. 2. Here, gapfilled DisALEXI-based MODIS retrievals at 500-m resolution have been fused with periodic ETd images from Landsat and ECOSTRESS using the Spatial Temporal Adaptive Reflectance Fusion Model (STARFM; Gao et al., 2006) to create ET datacubes with both medium spatial (30-m) and high temporal (daily) resolution. Comparisons of datacubes constructed with Landsat only and with Landsat+ECOSTRESS against flux tower observations are used to identify value added by the additional thermal temporal sampling. The multi-source ET data fusion process and gap-filling processes are described in greater detail by Sun et al. (2017) and Yang et al. (2017).

3.3. Data

3.3.1. Model inputs

Inputs to DisALEXI include remotely sensed surface data (LST, LAI and albedo), sub-daily meteorological forcings (insolation, air temperature, vapor pressure, atmospheric pressure and windspeed) from the Climate Forecast System Reanalysis (CFSR; Saha et al., 2014), as well as daily CONUS-wide ALEXI ETd maps at 4-km resolution used as the baseline for disaggregation (Sun et al., 2017; Anderson, 2018) (Fig. 2). Construction of gap-filled moderate resolution MODIS 500-m ETd timeseries used as the datacube fusion backbone (right side of Fig. 2) is described by Yang et al. (2018). In this section we focus specifically on preprocessing of medium-resolution remote sensing inputs for Landsat and ECOSTRESS disaggregation; in particular, remotely sensed TIR images for LST retrieval and VSWIR data for constructing 30-m LAI and albedo model inputs.

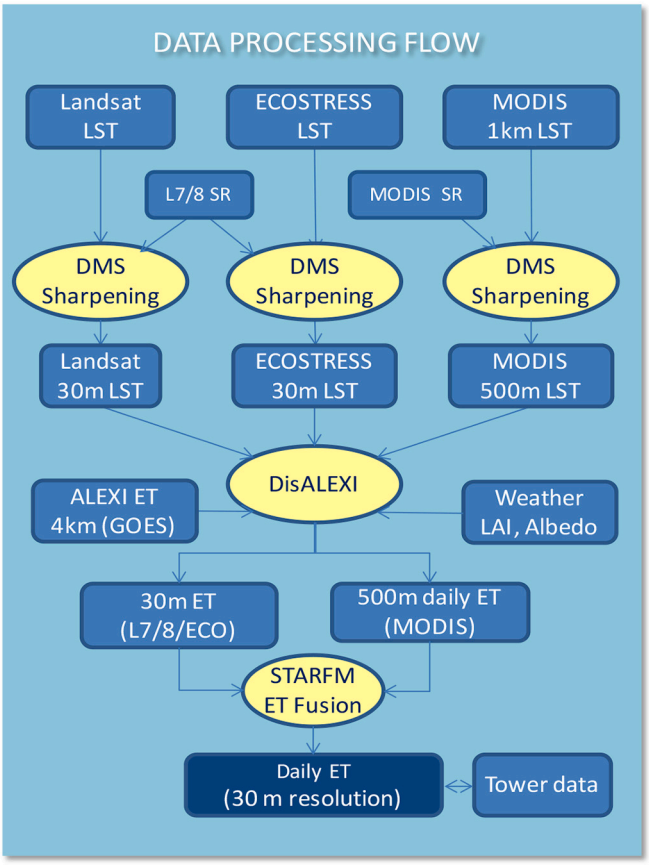

Fig. 2. Schematic summarizing the processing flow used to generate daily 30-m ET datacubes over target modeling sites.

3.3.2. TIR inputs

For Landsat disaggregation, thermal imagery from Landsat 7 (L7) band 6 (low gain) and Landsat 8 (L8) band 10 were used, spanning the full year of 2018. Collection 1 Level-1 thermal band products were downloaded from USGS. To facilitate multi-band usages, the USGS Land Product Generation System (LPGS) resamples Landsat thermal data to a 30-m grid commensurate with the VSWIR band products using a bicubic convolution method. At-sensor brightness temperatures were atmospherically corrected to surface brightness temperature using MODTRAN (Berk et al., 1998), and then emissivity corrected as implemented in the prototype USGS Landsat LST processing system (Cook et al., 2014). Atmospheric profile data used in the atmospheric correction were obtained from the Modern-Era Retrospective analysis for Research and Applications (MERRA-2) dataset (Gelaro et al., 2017). The sun-synchronous orbit of Landsat constrains image collection to around 10:30–11:00 a.m. local time (LT) for the range of latitudes sampled in this study, while 185-km swath width confines viewing angle to near nadir (<7°).

ECOSTRESS was launched on June 29, 2018 and installed on the ISS on July 5, 2018. Post-checkout, usable data were acquired in 2018 between August 20 (start of mission) and September 9, and in 2019 between January 4 and March 14. Each of the two data breaks represent a temporary pause in science acquisitions to investigate the failure of primary and backup mass storage devices. The instrument firmware has since been reconfigured to enable direct data streaming, and ECOSTRESS has been streaming uninterrupted data since May 15, 2019. In this study we use 2018 imagery acquired between DOY 200–280, defined hereafter as the "ECOSTRESS era". Level 2 land-surface temperature and emissivity (LST&E) and cloud mask swath products (ECO2LSTE and ECO2CLOUD) and Level 1 geolocation information are available for download from the USGS Land Processes Distributed Active Archive Center (LP DAAC; https://lpdaac.usgs.gov/). Level 3 USDA-DisALEXI ET products can also be obtained from the LP DAAC over targeted U.S. agricultural sites.

The ECOSTRESS LST&E swath data were gridded to geographical coordinates using the Elliptical Weighted Averaging (EWA) algorithm in the pyresample python library, while the discrete cloud class data were gridded using nearest neighbor via kd_tree. All products were then resampled to the 30-m UTM grid commensurate with the Landsat products over each modeling domain using nearest neighbor. Several other gridding approaches were tested, including cubic convolution and direct resampling to the 30-m WRS grid, all giving similar results. ECOSTRESS LST and emissivity are derived with the Temperature Emissivity Separation (TES) technique (Gillespie et al., 1998) using radiances collected in 5 spectral window bands between 8 and 12.5 μm, as described in the ECOSTRESS Level 2 LST&E ATBD (Hulley and Hook, 2018b). In this approach, one single state surface temperature and spectral emissivity values for each band are separated from the multi-band thermal radiances, with atmospheric compensation iteratively achieved using the Radiative Transfer for TOVS algorithm (RTTOV; Saunders et al., 2018) with input atmospheric profiles from the low latency Goddard Earth Observing System (GEOS) Model, Forward Processing (FP) (https://gmao.gsfc.nasa.gov/GEOS_systems/). The ISS orbit affords image collections at varying times, both night and day, and sometimes multiple acquisitions in a single day at higher latitudes. In this study, our testing has been constrained to daytime overpasses between 7:00–17:00 LT (noon + − 5 h). The ECOSTRESS swath width (nominally 402 km) extends to view angles of ±26°, and data at all view angles are evaluated. The Level 2 cloud product (Hulley and Hook, 2018a) was used to screen cloud impacted pixels, masking all pixels classified as cloud over land and water pixels. Pixels in identified region-growing buffers around clouds (bit field 1 in the ECOSTRESS L2 Cloud product) were retained in this analysis since additional masking of

buffers led to large loss of usable pixels within the modeling domains. The cloud mask provides both buffered and unbuffered cloud mask options for users depending on the degree of uncertainty that can be tolerated.

3.3.3. VSWIR inputs

VSWIR inputs (LAI and albedo) at 30-m resolution for both Landsat and ECOSTRESS disaggregation were constructed from Landsat Collection 1 surface reflectance (SR) data. LAI is generated with a sample-based machine learning approach using samples from the 500-m MODIS Collection 5 MCD15A3H LAI product and Landsat SR in the green, red, NIR, and SWIR bands (Gao et al., 2012a). Albedo was computed with the narrow-to-broadband conversion equation developed for Landsat SR bands by Liang (2000).

All L7 and L8 thermal images with cloud cover <80% were processed as defined in the pixel_qa band. Landsat-based ET disaggregation used same-day LST, LAI and albedo inputs. Because ECOSTRESS is a thermal-only instrument, VSWIR inputs (LAI and albedo) for ECOSTRESS disaggregation were taken from a contemporaneous Landsat overpass. To select this Landsat overpass, all available L7 and L8 scenes were triaged and scenes with minimal clear-sky coverage (<50%) were removed from consideration. The scene collected closest to the ECOSTRESS acquisition date was used to create VSWIR inputs for that date. While L7 data are impacted by striped gaps resulting from the scan-line corrector (SLC) failure in 2013, it was decided that the benefits of reducing temporal separation between TIR and VSWIR inputs achieved by including L7 overpasses outweighed the drawbacks. Gaps in ECOSTRESS ET retrievals represent the union of gaps (clouds and SLC) in the ECOSTRESS LST and paired Landsat VSWIR acquisitions.

3.3.4. Thermal sharpening and TIR/VSWIR registration

L7, L8 and ECOSTRESS TIR images have varying native resolution between ~60-100 m, significantly coarser than that of the 30-m Landsat VSWIR model inputs. To bring all TIR and VSWIR inputs to a common 30-m resolution for datacube construction, we utilized the Data Mining Sharpener (DMS) algorithm of Gao et al. (2012b). Similar to the Landsat LAI method, DMS also uses regression trees - in this case constructed at the coarser TIR resolution using spatially aggregated SR values in multiple spectral bands and TIR samples, then applied to the SR data at 30-m. In a final "energy conservation" step, the sharpened and original maps are compared at a scale close to that of the native TIR resolution and residuals are computed. This residual map is then re-introduced into the sharpened TIR to ensure that it reaggregates to the original map at this energy conservation scale. The energy conservation scale used for sharpening L7 and L8 TIR imagery is 60 and 90 m, respectively.

Temporally varying registration accuracy of the ECOSTRESS products and variations of spatial resolution with sensor view angle necessitated relaxation of the scale of energy conservation for ECOSTRESS thermal sharpening - from the nominal native resolution of 70 m (at nadir) to ~180 m (Xue et al., 2020). While this results in some effective loss of spatial information in thermal variability, relaxation was found to be critical to maintaining consistency in TIR and VSWIR model inputs to the TSEB. Despite the relaxation, some artifacts of TIR-VSWIR misregistration persist especially at large ECOSTRESS view angles, as discussed in Sec 4.3.

3.3.5. Flux datasets

This study used data from 12 flux towers across the U.S. located in cropped fields within the target ET modeling domains (Table 1) to evaluate the accuracy of modeled daily fluxes and the improvement achieved with additional temporal sampling of ECOSTRESS. Each tower was equipped with an eddy covariance (EC) system measuring turbulent fluxes of sensible and latent heat, along with net radiometers and multiple soil heat flux sensors. Common EC instrumentation include 3-dimensional sonic anemometers, sonic temperature sensors, and open-path infrared gas analyzers for water vapor and CO_2. Daily ET is computed from the daily integrated latent heat flux as in Sec. 3.1.

The three California domains support GRAPEX study objectives and include four towers in irrigated vineyards used in this study, each with similar instrumentation described by Alfieri et al. (2019). The RIP760 tower is in a Chardonnay vineyard within the Ripperdan production area near Madera, CA, maintained by E&J Gallo Winery (Ripperdan domain). The Sierra Loma domain includes the seminal GRAPEX towers in adjacent Pinot noir vineyards outside Lodi, CA. These towers were formerly known as Lodi1 and Lodi2, but under new GRAPEX naming conventions are now referred to using their vineyard block name (Sierra Loma) as SLM001 and SLM002. The BAR012 tower is sited in a Cabernet Sauvignon block in the Barrelli Creek ranch outside Cloverdale, CA.

The Sierra Loma domain also covers part of the California Delta – a major irrigation district at the San Joaquin and Sacramento River confluence. Several AmeriFlux towers are maintained by UC Berkeley in the Delta to study soil subsidence and greenhouse gas emissions in Delta croplands, as well as the biophysical evolution of restored wetlands (Eichelmann et al., 2018). In this study, we use data from two towers in irrigated fields on Bouldin Island: US-Bi1 in alfalfa and US-Bi2 in corn, established in late-2016 to mid-2017 (Hemes et al., 2019).

The three Corn Belt domains contain several long-term Ameriflux towers in corn and soybean rotation. Mead includes long-term Ameriflux sites in irrigated (US-Ne1 and US-Ne2) and rainfed (US-Ne3) fields (Suyker et al., 2004), all in close proximity to Mead, NE. These towers are part of the USDA-ARS PHRP LTAR. Ameriflux sites US-Br1 and US-Br3 are the UMRB LTAR south of Ames, IA, sampling side-by-side rainfed fields. The Bondville domain includes the long-term US-Bo1 AmeriFlux tower in a rainfed field outside Bondville, IL (Meyers and Hollinger, 2004). While not formally part of LTAR, this tower is located within the LMRB LTAR region.

Finally, two towers in the USDA-ARS LCB LTAR site in Maryland were used, both in fields planted in soybean in 2018. The OPE3 flux tower is located in Beltsville, MD, while the Choptank tower is in Caroline County on the eastern shore of Maryland.

Standard corrections, including coordinate rotation and Webb-Pearman corrections for buoyancy and water vapor density fluctuations, were applied to EC flux timeseries collected at each site (see e.g., Alfieri et al., 2019). Modeled daily fluxes were compared with tower observations both as measured and with a correction enforcing closure in the surface energy balance, providing a metric of uncertainty in the flux measurements (Twine et al., 2000). At most sites, a residual closure correction was applied to latent heat flux at the daily (24 h) timescale, assigning the full energy balance residual at the daily timescale to the latent heat flux (Prueger et al., 2005). In the case of the SLM sites, a shift in nighttime wind patterns was noted in 2018 such that overnight the towers sampled conditions from a neighboring vineyard to the east that had significantly lower canopy cover. For these two towers, the 24 h closure-corrected latent heat flux was computed as the daytime residual augmented by the difference between 24 h and daytime observed latent heat. Assuming optimal conditions (best management practices followed in site selection and instrument deployment and maintenance), accuracies in EC measurements of ET at daily timesteps have been reported to be on the order of 10–15% (Allen et al., 2011; Kustas et al., 2015; Mauder et al., 2018).

4. Results

Daily 30-m ET datacubes were constructed at each flux site by fusing daily MODIS 500-m ETd with Landsat ETd data layers (Landsat only) and with both Landsat and ECOSTRESS ETd retrievals (Landsat+ECOSTRESS). We use these datacubes to investigate how well the model results from each sensor agree with the flux tower observations on overpass dates, how inter-consistent the Landsat and ECOSTRESS retrievals are both spatially and temporally, and under what conditions the additional ECOSTRESS retrievals improved the accuracy of the modeled daily ET timeseries. In particular, we investigate model

performance in terms of impacts of ECOSTRESS temporal sampling, view angle, overpass time, and time separation between TIR and VSWIR data acquisitions, as detailed below.

4.1. Comparison with flux tower observations

Annual time-series plots of daily ET observed at the tower sites (both with and without closure corrections) are shown for 2018 in Fig. 3a along with modeled daily ET generated via data fusion using Landsat only and Landsat+ECOSTRESS. Direct remote sensing retrievals on usable/fillable Landsat and ECOSTRESS overpass dates anchoring the fusion are also indicated. In general, the Landsat and ECOSTRESS retrievals are temporally consistent with each other at most of the flux sites, with some exceptions. Possible sources of inconsistency are investigated further in following sections.

To quantify the value added by ECOSTRESS, we compare the performance of ET retrievals at daily and weekly timesteps generated via data fusion with and without ECOSTRESS (Fig. 4; Table 2). Over the 2018 ECOSTRESS image acquisition period (day of year [DOY] 200–280), root-mean-square errors (RMSE) for all sites combined improved slightly with ECOSTRESS - from 1.24 to 1.18 mm d^{-1} at daily timesteps and from 1.01 to 0.94 mm d^{-1} for weekly average ET (Fig. 5). Over the full year, the performance was similar with and without ECOSTRESS due to the short period of data availability in 2018, with RMSE of 1.0 (0.8) mm d^{-1} at daily (weekly) timesteps. Despite the small impact on statistics from all sites combined, a few individual sites showed unique sensitivity to the improved temporal sampling as discussed below.

4.2. Temporal sampling

At the central California flux sites (Ripperdan, Sierra Loma, and Bouldin Island), there was typically sufficient clear-sky sampling with L7 and L8 to capture major ET changes (Fig. 3a). One exception is US-Bi1, where monthly cuttings of the alfalfa crop results in multiple peaks in ET through the growing season. An additional sample around DOY 160 would have facilitated better definition of the June peak; however, this was prior to the launch of ECOSTRESS. ECOSTRESS did not improve temporal reconstruction at the alfalfa site during the ECOSTRESS era, which may be due in part to non-simultaneous TIR-VSWIR acquisition under conditions of rapid vegetation change, as discussed further in in Sec 4.6.

Further to the north in California, at the Barrelli site (BAR012), errors in daily and weekly flux retrieval improved by 25% and 55%, respectively, with the additional ECOSTRESS sampling. ECOSTRESS ETd on DOY 223 and 239 were superior to the Landsat values and their inclusion improved biases during adjacent periods. In particular, the additional samples between DOY 233 and 243 helped to better define a reduction in weekly ET after irrigation ceased (see Fig. 3a).

Outside of California (Fig. 3b), the site that benefited most from ECOSTRESS was OPE3 in the eastern United States, where frequent cloud cover can severely limit seasonal ET retrievals based on Landsat alone. At this site, daily and weekly RMSE values were reduced by 30% and 40%, respectively, by including the additional ECOSTESS samples (Fig. 4). These samples effectively filled a large gap in mid-year Landsat coverage due to persistent cloud cover on Landsat overpass dates (Fig. 6). No Landsat scenes with sufficient coverage to be used in the fusion process were acquired between DOY 197–277 (16 July – 4 October). This constituted nearly the full growing season for the soybean crop at OPE3, from shortly after emergence to mid-senescence (Fig. 6). Four additional ECOSTRESS samples during this period significantly improved accuracy of daily timeseries, reducing RMSE from 1.6 to 1.1 mm d^{-1} over the ECOSTRESS imaging period and from 1.1 to 0.8 mm d^{-1} over the full year. All three ECOSTRESS retrievals used VSWIR inputs from a Landsat acquisition during an off-peak time, DOY 269, when the crop had already started to senesce. The lower LAI from that day may contribute to underestimation of transpiration fluxes on the ECOSTRESS dates, whereas a clear VSWIR acquisition near peak greenness would have increased ETd estimates during that interval toward values reflected in the closed tower observations.

ECOSTRESS did not significantly change STARFM results at most of the Choptank, Bondville, Mead or Ames flux sites, even though these sites had large gaps in Landsat coverage due to cloud cover (Fig. 3a,b). At each of these sites, a clear Landsat retrieval was available near peak crop biomass, serving to anchor the fused ET timeseries during the latter part of the growing season. RMSE over the ECOSTRESS era increased at the rainfed USNe3 site with the addition of ECOSTRESS, largely due to a single ECOSTRESS retrieval on DOY 234 which served to decrease fluxes at this site by 1.4 mm d^{-1} on average over the surrounding two-week interval. The region over the three Mead flux sites was cloudy and gap-filled on this day, resulting in a degraded ET estimate at USNe3. Additional clear thermal image acquisitions during this interval would have helped the fusion system recover more quickly from this single poor retrieval; thus, noise reduction is another benefit of frequent thermal sampling.

4.3. View angle

Sensor view angle was identified as a source of additional uncertainty in SEB-based ECOSTRESS ET estimation. While the Landsat swath is constrained to ±7° from nadir, the swath for ECOSTRESS has been expanded to ~ ±26° to improve temporal revisit. Visual inspection of the 2018 scenes processed suggests that the effective resolution of the L2 ECOSTRESS LST product is somewhat lower than that of L8 at nadir, although the nominal resolution cited for ECOSTRESS (70 m) is higher than that for L8 (100 m). The resolution of the ECOSTRESS LST degrades with increasing view angle, as expected for a whisk-push imaging system. Fig. 7 shows a comparison between LST at native resolution from ECOSTRESS and L8 over a range of view angles, extracted from subsites in the Sierra Loma domain on DOY 216. Field-scale features in the ECOSTRESS sub-scenes are progressively blurred at larger view angles, particularly at angles exceeding 20°.

Thermal sharpening using the DMS package helps to enhance the spatial consistency between ECOSTRESS and Landsat LST at all view angles, improving the “stackability” of the multi-source thermal imagery. Due to the relaxed energy conservation scale used to accommodate ECOSTRESS geolocation errors (Sec. 3.3.2), DMS output for ECOSTRESS LST may in fact even appear slightly “sharper” than for Landsat, although at the expense of true thermal spatial information content (Fig. 7). Above 20°, however, degradation in thermal pixel size and VSWIR/TIR co-registration lead to artifacts in the sharpened LST and resulting ET retrievals. These artifacts are manifested as a blurring or bleeding of LST signals over discrete feature boundaries (see e.g., sharpened ECOSTRESS LST tile at 20° in Fig. 7). Fig. 8 compares ETd from three direct ET retrievals over a period of 4 days (246–250), extracted over the Sierra Loma tower sites. ECOSTRESS ETd on DOY 246 (11.6°) is similar in quality to Landsat ETd on DOY 248, while ECOSTRESS on 250 (23.2°) shows signs of degraded VSWIR/TIR spatial correspondence both in the sharpened LST and in the ETd output. These artifacts are particularly notable at the sharp discontinuity between irrigated vineyards and the senesced rainfed grassland along the northwest edge of the agricultural zone mid-scene. Note that identification of these artifacts required visual inspection – they may or may not be detectable in time series extractions. For example, the ECOSTRESS estimated ET at the SLM001 tower site on DOY 250 is only slightly elevated (0.3 mm d^{-1}) in comparison with the Landsat ET two days prior.

4.4. Overpass time

Another potential source of inconsistency in daily ET retrievals from Landsat and ECOSTRESS is the thermal sensor overpass time. While L7

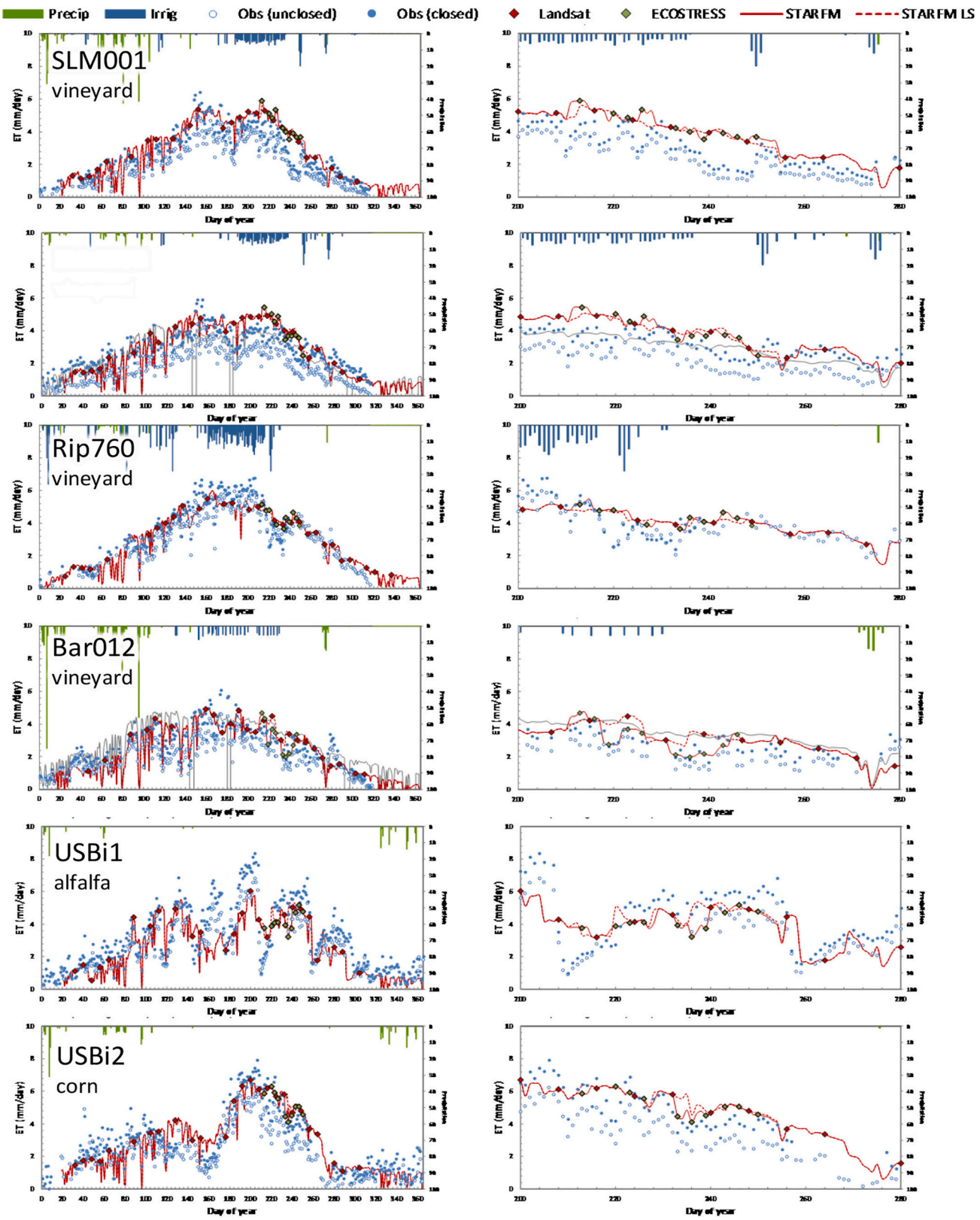

Fig. 3a. Model – measurement time-series intercomparison at the CA flux tower sites for the fully year of 2018 (left) and the ECOSTRESS era (DOY 200–280; right). Dotted red lines indicate STARFM results based on Landsat only, while solid red lines show results using Landsat+ECOSTRESS. Red/green diamonds indicate direct ETd retrievals by Landsat/ECOSTRESS, while closed and unclosed daily ET observations are plotted as filled and unfilled blue circles, respectively. Precipitation and irrigation (where known) are shown as green and blue bars. (For interpretation of the references to colour in this figure legend, the reader is referred to the web version of this article.)

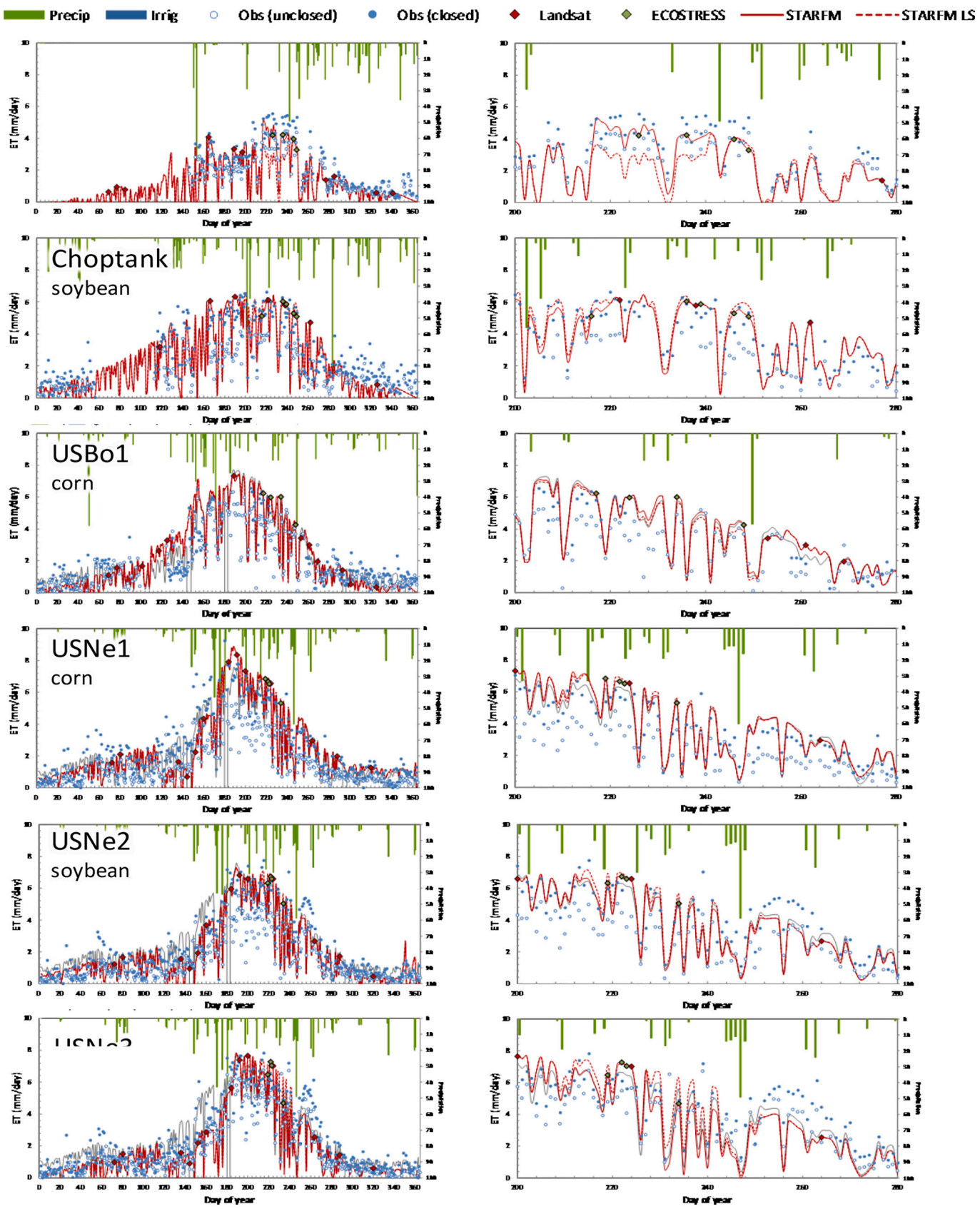

Fig. 3b. Model – measurement time-series intercomparison at the MD, IL and NE tower sites.

Table 2
Statistical metrics of model performance (RMSE) for estimating ET (mm d^{-1}) at daily and weekly timesteps with Landsat only (L) and Landsat+ECOSTRESS (L + E), over the full year and the 2018 ECOSTRESS era (DOY 200–280). N is the number of daily flux observations available over the prescribed interval.

		Full year			ECOSTRESS era		
Timescale	Tower	N	RMSE L	RMSE L + E	N	RMSE L	RMSE L + E
DAILY	slm001	214	0.88	0.89	69	1.18	1.22
	slm002	193	0.93	0.93	70	1.08	1.07
	USBi1	266	1.37	1.39	71	1.35	1.41
	USBi2	215	1.05	1.02	53	1.23	1.12
	rip760	170	0.85	0.86	39	1.01	1.01
	bar012	211	0.84	0.78	51	0.98	0.74
	USNe1	316	1.23	1.22	75	1.47	1.45
	USNe2	306	0.92	0.90	73	1.13	1.06
	USNe3	324	1.02	1.04	80	1.34	1.42
	USBo1	170	1.13	1.13	28	1.24	1.28
	chop	258	0.97	0.96	78	0.97	0.93
	ope3	139	1.12	0.83	56	1.60	1.07
	ALL	2782	1.05	1.03	743	1.24	1.18
WEEKLY	ALL	353	0.84	0.82	96	1.01	0.94

and L8 are in sun-synchronous orbit with overpass time generally around 10:30 a.m., the ISS orbit provides overpass at varying time of day, and sometimes multiple times per day. Since the thermal image used in DisALEXI defines the spatial structure in the 30-m ETd map, time-of-day of acquisition can impact the resulting retrieval. The 2018 Landsat and ECOSTRESS combined ETd timeseries were inspected to determine a recommended window for usable overpass times, and to identify dependency of ET structure on TIR image acquisition time.

Using the time series extracted at the SLM001 tower in Fig. 8 as an example, ETd derived from LST retrieved at overpass times ranging between 8 a.m. and 4 p.m. are reasonably consistent over time, except for the collections at large view angle as noted in Sec. 4.3. This may be due in part to the fact that this vineyard is irrigated, resulting in a more symmetrical diurnal thermal curve pre- and post-noon. The DisALEXI energy conservation step, which enforces aggregation to the ALEXI baseline ETd flux at the 4-km scale, also reduces sensitivity to high-resolution LST acquisition time. Still, 30-m DisALEXI flux distributions within the disaggregated ALEXI pixel footprint (4-km) are strongly dependent on temporally varying high-resolution LST patterns from different acquisition times, even on the same day. In addition, surface moisture and vegetation stress conditions can vary over the course of the day, leading to a different perspective on daily ET at field scale depending on time of image acquisition.

Visual inspection revealed that, in many cases, retrievals based on early morning ECOSTRESS LST were overly uniform due to reduced surface temperature variability expressed under low morning solar radiation load. This is demonstrated in a comparison of ECOSTRESS (8:45 a.m.) and Landsat (10:38 a.m.) ETd retrievals with DisALEXI on 6 Sept

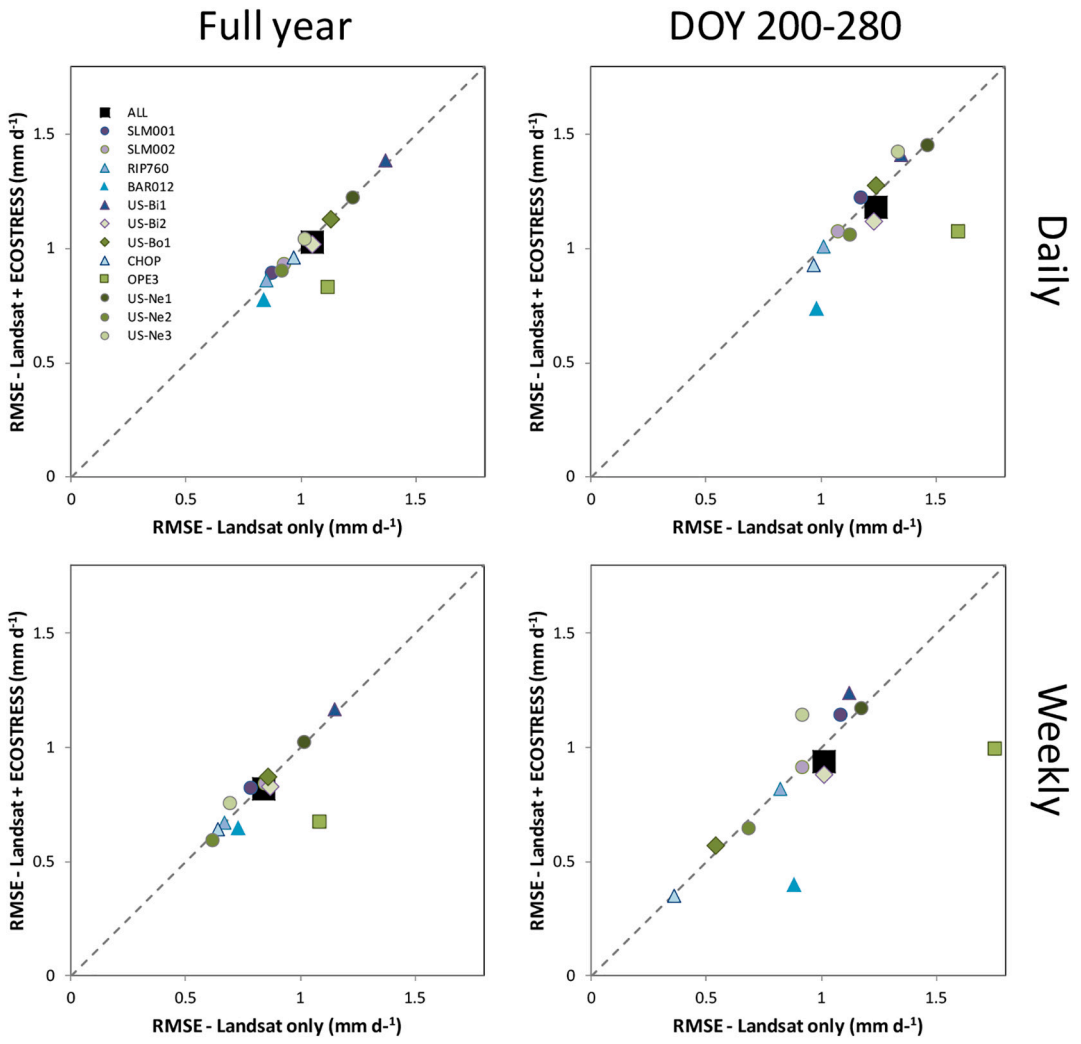

Fig. 4. Comparison of RMSE in daily (top) and weekly (bottom) ET developed with and without ECOSTRESS over the full year (left) and 2018 ECOSTRESS era (right).

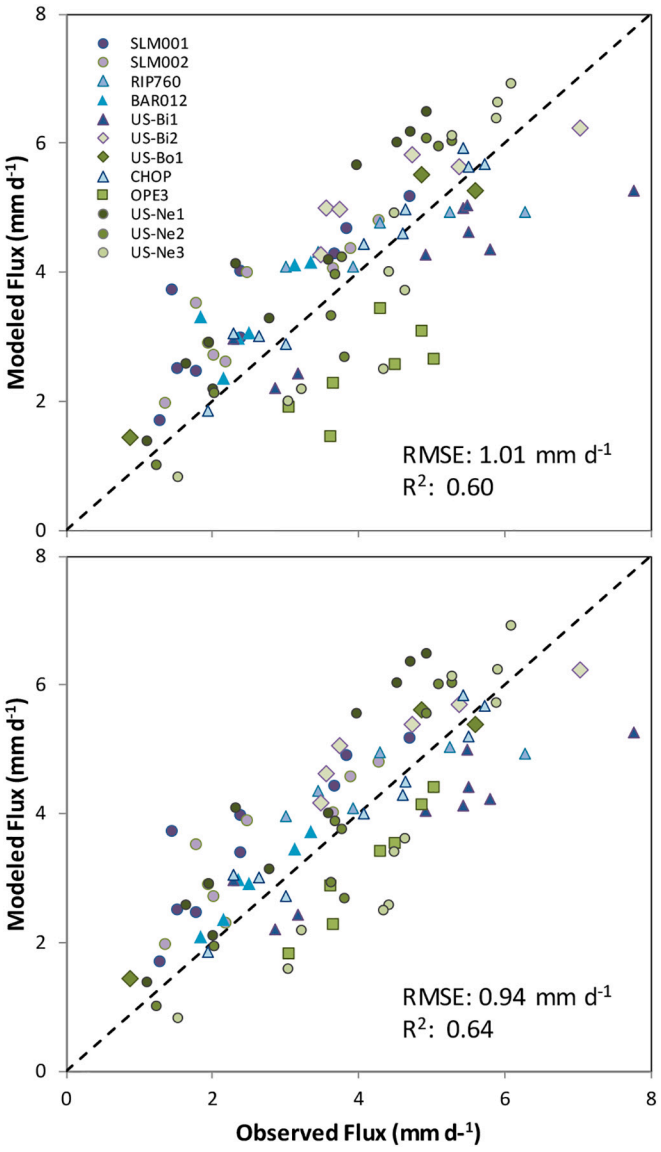

Fig. 5. Comparison of measured 7-day average fluxes during the 2018 ECOSTRESS era with modeled fluxes generated via data fusion with Landsat only (top) and with Landsat+ECOSTRESS (bottom). Inclusion of ECOSTRESS primarily benefited sites BAR012 and OPE3 over this period.

(DOY 249) around the RIP760 tower site in Fig. 9 (top row), showing subset regions of 9 × 9 km, or about 2 × 2 ALEXI pixels in scale. Histograms of fluxes over the two image subsets demonstrate a larger contrast in fluxes from the Landsat LST data acquired closer to noon, with fallow fields appearing drier in the Landsat retrieval and higher ET in irrigated fields. Despite the clear differences in spatial patterns, the ET extracted within the vineyard at the tower site is similar in both retrievals (4.1 and 3.9 mm d^{-1} for Landsat and ECOSTRESS, respectively). This sub-scene was also acquired at high view angle (24°), contributing to blurring at field edges. While early morning LST may not be optimal in isolation, pairing with a same-day near-noon high-resolution LST image from Landsat could enable time-differential applications of TSEB at field-scale (e.g., Kustas et al., 2001; Guzinski et al., 2013).

The impact of early morning LST on ET retrieval is also seen in the 3-day sequence (24–27 August; DOY 236–239) at the Choptank site shown in Fig. 10. The Choptank flux tower is located in a cropped field (soybean in 2018) within a crop/forest mosaic landscape. Although the time-series extracted at the tower site appears consistent between dates (Fig. 3a,b), with values of 5.8–6.0 mm d^{-1}, visual inspection reveals that the retrieval using the ECOSTRESS LST image at 7:09 a.m. LT on DOY 236 does not capture the expected variability in ET between the forest and crop patches. Landsat (DOY 238) and ECOSTRESS (DOY 239) ETd maps based on LST acquired at 10:30–12:30 LT more realistically depicted the expected patterns.

In contrast, ET fluxes retrieved from ECOSTRESS LST acquired in the early afternoon tended to be similar in pattern and distribution to Landsat-derived ETd. Fig. 9 also shows image subsets over Sierra Loma and Bouldin Island on 4 August (DOY 216) and Ripperdan on 5 August (DOY 217), when there were same-day overpasses of Landsat at 10:45 and ECOSTRESS at 14:00–15:00. Flux histograms are similar from both sensors but with some shifting between modes in the distribution, enhancing the lower mode (aqua-to-light green tones) in the afternoon retrieval. Contrasts are enhanced as well. Well-irrigated fields over the Sierra Loma site have higher ET by ~0.5 mm d^{-1} with the afternoon ECOSTRESS LST acquisition, while the large bare field in the northwest corner of the Bouldin Island scene in Fig. 9 appears drier by about the same amount. Note there is some bleeding of fluxes around this discontinuity due to TIR-SR misregistration and thermal sharpening artifacts. In some cases, ET changes within-day may indicate active water management. For example, the difference map for the subset NW of the Ripperdan flux site shown in the bottom row of Fig. 9 identifies a field with a strong change signal of ≥4 mm d^{-1}, which may have been irrigated between the Landsat and ECOSTRESS overpass times. Further analysis is required to define thresholds distinguishing real within-day change from false signals due to inter-sensor differences in resolution and registration.

4.5. Cloud cover

ECOSTRESS overpass time was also found to impact the percentage of usable cloud-free data within the target modeling domains. The optimal overpass timing in terms of clear-sky probability is geographically variable, determined by local cloud cover climatology (Whitcraft et al., 2015). In the scenes evaluated in this study there were some cases where the ISS orbit afforded multiple site overpasses in one day, facilitating a qualitative analysis of diurnal changes in cloud coverage. Two cases demonstrating different time behaviors in terms of cloud cover are shown in Fig. 11.

Early morning LST acquisitions at the Barrelli site in Sonoma County, CA, were often impacted by early morning fog that was not flagged in the ECOSTRESS cloud mask, being difficult to detect with thermal-only data. Early fog is also frequently observed on the ground during GRAPEX field campaigns, tending to burn off by the time of the late-morning Landsat overpass. The fog layer results in an overly smooth ET distribution, as demonstrated in comparisons of ETd retrievals on August 21 (DOY 233) from LST acquisition at 8:14 and 14:43 LT.

In contrast, at the more humid sites in the Midwest and in Maryland, cloud cover more often occurred in afternoon ECOSTRESS acquisitions, likely due to convection – an example from August 24 (DOY 236) over the Choptank domain is also shown in Fig. 11. The 7:09 LT LST acquisition was largely cloud-free, with gaps in the associated ETd map primarily due to scan-line corrector gaps and clouds occurring in the L7 SR dataset used as input. These gaps were readily gap-filled using the STARFM-based approach described by Yang et al. (2017) (see Fig. 11). The ETd map derived from the 15:37 ECOSTRESS overpass, however, shows extensive contamination from small convective clouds. The ECOSTRESS L2 cloud mask does not explicitly model cloud shadows, resulting in this case in a map that cannot be easily gap-filled. Implementation of the cloud buffer and morphological filling option in the mask does flag these cloud shadows, but also removes most of usable clear pixels in this scene. Limitations in the ECOSTRESS cloud-masking strategy, by necessity based on TIR bands only, are discussed further in Sec. 5.2.

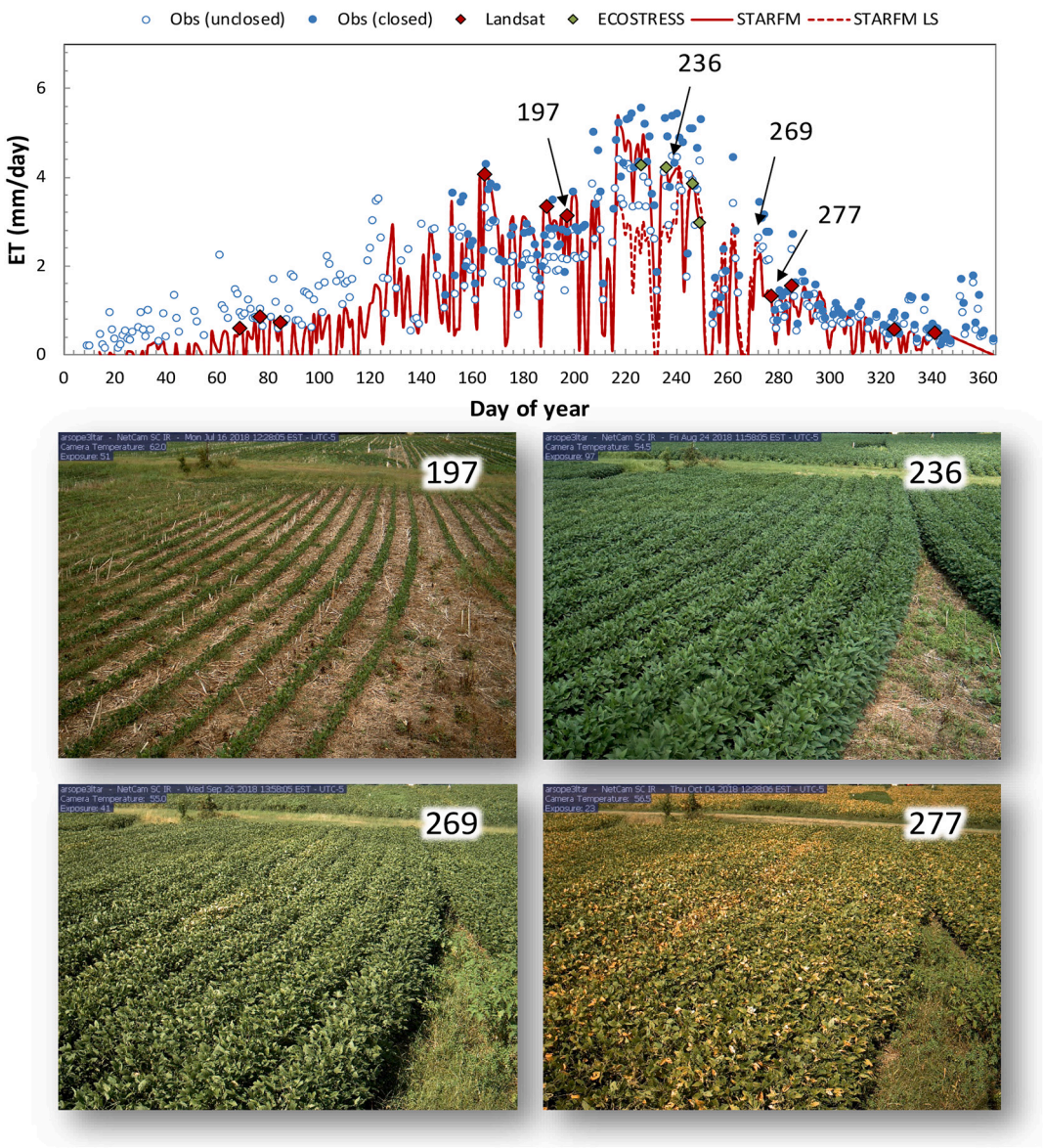

Fig. 6. Model – measurement intercomparison at the OPE3 tower site (MD) as in Fig. 1. Photographs are from a phenocam in OPE3 and show soybean canopy conditions on key dates highlighted in the upper panel.

4.6. TIR-VSWIR temporal separation

The time separation between acquisition of TIR and VSWIR inputs used in DisALEXI was 5 days on average for all 2018 ECOSTRESS images processed, with 2-day typical separation in CA and 12 days for the eastern IL and MD sites. Separation can have a significant impact on TSEB or other energy balance algorithms that require consistent information regarding land-surface temperature, surface albedo, and vegetation cover amount.

Impacts of TIR/VSWIR mismatch on TSEB ET retrievals are demonstrated in Fig. 12 over a set of alfalfa fields due north of US-Bi1. Alfalfa fields are typically harvested in this region on a monthly basis and regrowth is rapid between cuttings; therefore, there is a high likelihood that non-simultaneous collection of TIR and VSWIR inputs will result in sampling of significantly different surface conditions. Based on Landsat surface reflectances and derived LAI, it is clear in Fig. 12 that a harvest occurred in this field between the L8 overpass on DOY 232 and the L7 overpass on DOY 240. This was confirmed with temporally dense VI timeseries derived from Planet Labs imagery (not shown). The higher temperatures in this field in the ECOSTRESS LST product for DOY 239 are consistent with post-cutting field conditions. If the ECOSTRESS LST image on DOY 239 (high LST) is processed using the LAI map from pre-cutting (DOY 232; high LAI ~3.5), the TSEB assumes the presumed fully vegetated canopy is severely stressed and transpiration is completely cut off, leading to anomalously low ET close to 0 mm d^{-1}. This phenomenon is also evidenced in several nearby fields that were harvested between DOY 232 and 240 (see negative/positive features in the LAI/ET difference maps in Fig. 12). If the post-cutting LAI map (LAI < 1 in-field) from DOY 240 is used, the ET is more reasonable (1–2 mm d^{-1}) compared to fully vegetated surrounding fields (5–6 mm d^{-1}).

Considering all 2018 ECOSTRESS retrievals over all flux sites, Fig. 13 demonstrates the dependency of model error (MAE) in ETd based on days of separation between TIR and VSWIR data acquisitions. In general, the ET accuracy is highest when both inputs are collected on the same day, and errors increase with increasing temporal separation – more than doubling when the separation was greater than 5 days. Note that this analysis is based on a limited temporal and spatial sample. A longer ECOSTRESS record and additional tower sites will be required to determine functional dependency of ET retrieval error on separation timescale.

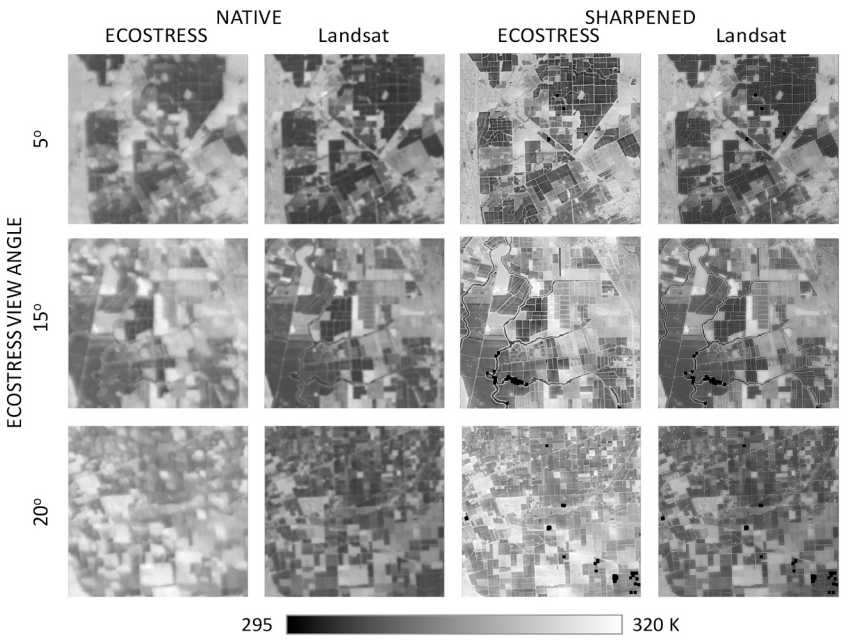

Fig. 7. Comparison of Landsat and ECOSTRESS LST at native and sharpened resolutions as a function of ECOSTRESS view angle, extracted from imagery acquired over the Central Valley, CA on DOY 216 at 10:30 (Landsat) 14:54 LT (ECOSTRESS). Black pixels in the sharpened images arise from the Landsat cloud mask, which has miss-classified small water bodies as cloud.

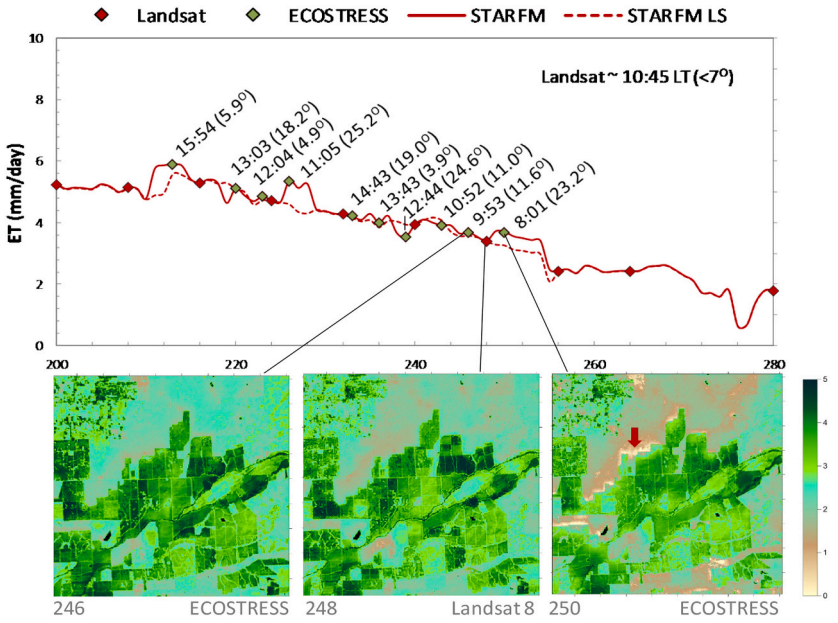

Fig. 8. Comparison of Landsat and ECOSTRESS ETd retrievals (mm d^{-1}) around the Sierra Loma tower sites over 4-day period, DOY 246–250. Times of LST acquisition (LT) are noted, as well as view angle of ECOSTRESS data (in parentheses). The red arrow in the DOY 250 ECOSTRESS ETd image (bottom row) indicates a discontinuity where sharpening artifacts are notable, as discussed in the text. (For interpretation of the references to colour in this figure legend, the reader is referred to the web version of this article.)

Temporal separation also has the impact of reducing the effective scene coverage for direct ET retrievals, which is defined as the union of the clear areas in both the TIR and VSWIR imagery. Maximum coverage is obtained when both waveband datasets are acquired simultaneously, while separation always serves to either maintain or reduce effective coverage. Impact of separation on the 2018 scenes analyzed here was assessed by comparing cloud-free area in the ECOSTRESS LST inputs to the combined cloud-free area in both LST and VSWIR inputs (Fig. 14). To avoid counting gaps imposed by the L7 scan-line corrector failure, the assessment was limited to dates processed with L8 VSWIR inputs. Coverage was reduced on average by 22% and up to 70% over these scenes. California scenes were least impacted due to lower cloud cover (11% reduction), while coverage over Corn Belt and Maryland domains was reduced by 30% on average.

5. Discussion

The power of ECOSTRESS lies in the opportunity it affords to explore, within the context of a low-cost research mission, new regions in medium-resolution thermal imager design space previously unsampled by the Landsat series. Findings from ECOSTRESS should be informative for developing applications-based requirements for future thermal IR satellite missions, including Landsat Next – the follow on to Landsat 9. The results in Sec. 4 demonstrate that ECOSTRESS thermal imagery can be used effectively and inter-operably with Landsat data to generate ET time series retrievals using SEB. Increased thermal imaging frequency at

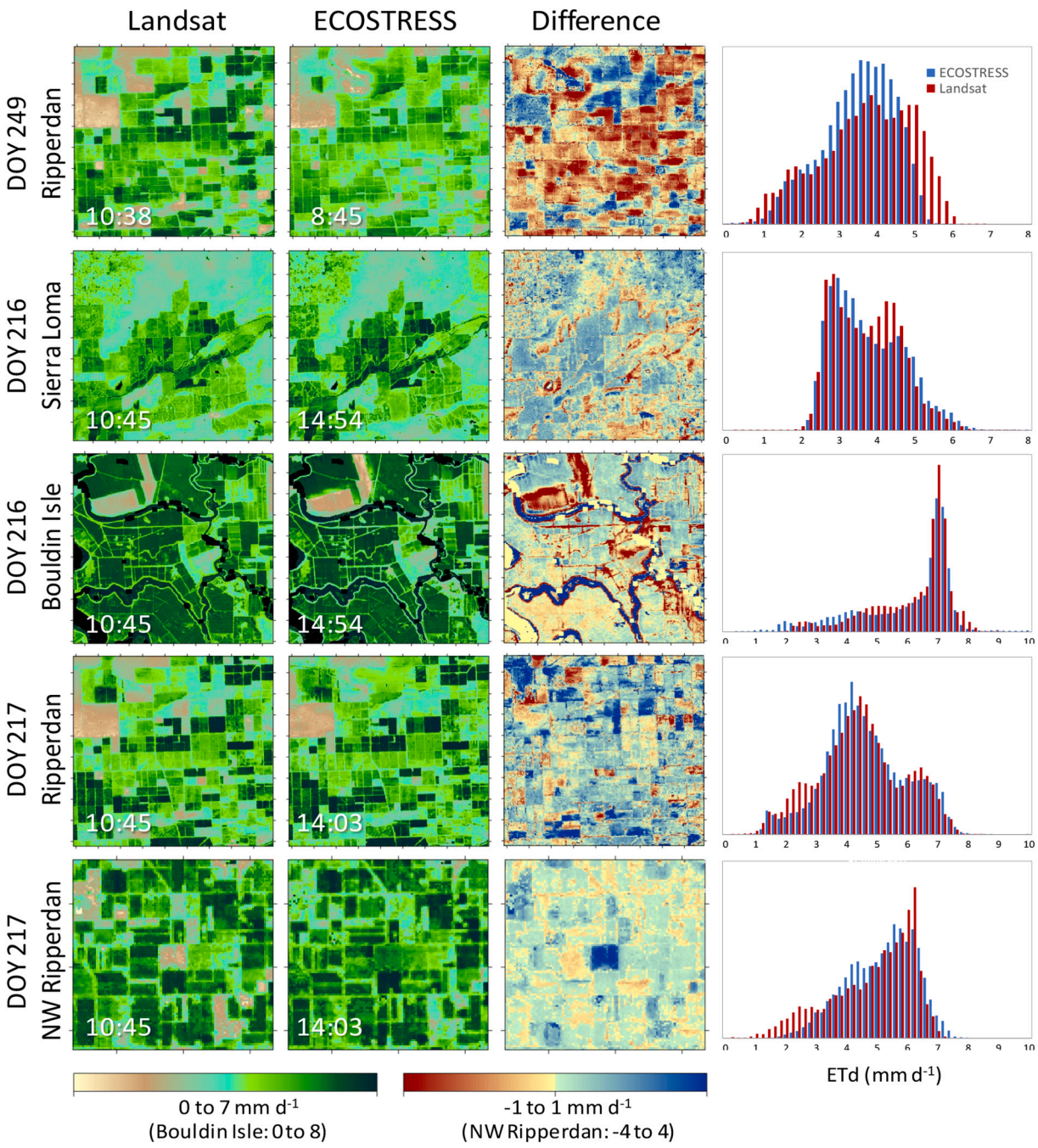

Fig. 9. Landsat and ECOSTRESS same-day ETd retrieval comparisons. Difference plots show ECOSTRESS minus Landsat ETd. Times of LST acquisition are noted. The ECOSTRESS Ripperdan sub-image for DOY 249 and NW Ripperdan for DOY 217 were acquired at a view angle of 24°, while the others were collected at around 16°.

Landsat scale will improve our ability to monitor and manage consumptive water use, particularly in areas with frequent cloud cover. These results also suggest constraints on ECOSTRESS acquisition time, view angle and spatiotemporal consistency with VSWIR inputs that may optimize its performance within SEB modeling systems.

The dual-source structure of TSEB and DisALEXI used here provides a stringent test on TIR/VSWIR input consistency, where physically incompatible LST and LAI inputs can lead to significantly anomalous ET retrievals. We note that other ET modeling systems may be differently sensitive to some of the issues identified here; for example, the Priestley-Taylor methods in PT-JPL show high sensitivity to VSWIR inputs but are less exacting in terms of requiring rigorous physical consistency between VSWIR and TIR inputs. While the STARFM method used here to interpolate between satellite overpass dates does influence model performance at daily timesteps (Table 2) to some extent, the constraints identified below are general and likely independent of interpolation method.

5.1. ECOSTRESS constraints for SEB modeling

In DisALEXI, TIR acquisitions between 9:00–17:00 local time generally produced reasonable ET patterns, while earlier overpasses often created flux distributions that were spatially too uniform. The utility of same-day early morning and pre-or post-noon LST image pairs from ECOSTRESS and Landsat could be exploited in DisALEXI using the dual-temperature-difference (DTD) method, whereby instantaneous fluxes at one time are bootstrapped to other times when thermal images are available (Norman et al., 2000; Kustas et al., 2001; Guzinski et al.,

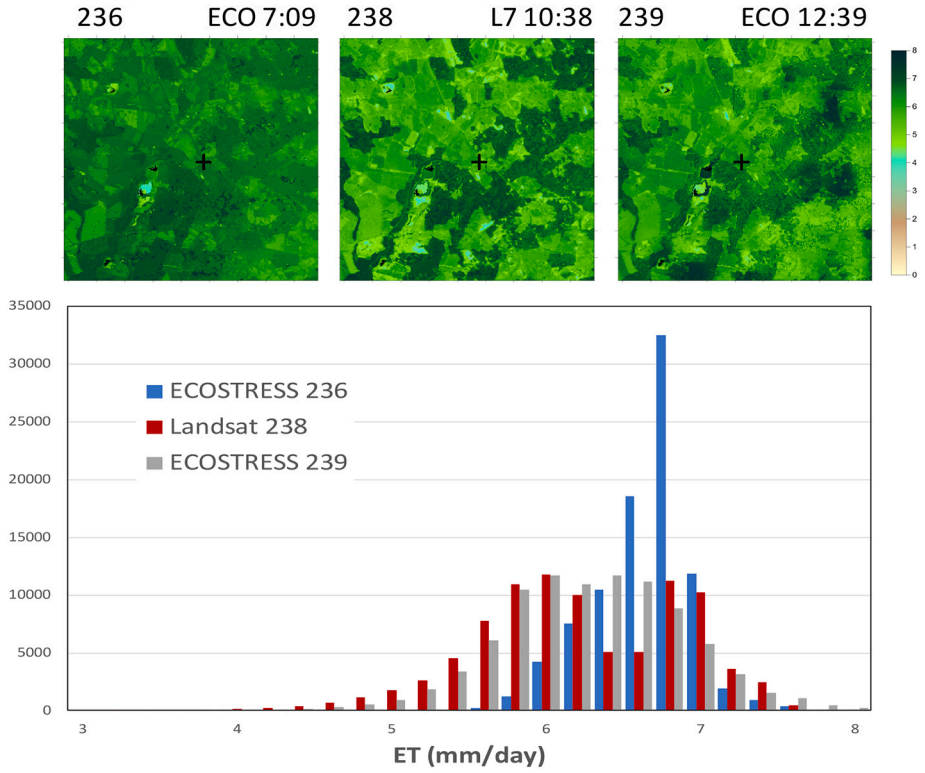

Fig. 10. Three-day ETd (mm d^{-1}) retrieval sequence over the Choptank flux site (indicated with +), and histogram of fluxes from each retrieval.

2013). Differences in morning and afternoon evaporative fraction could be a useful remote early indicator of developing vegetation stress, capturing impacts of midday stomatal closure under soil moisture limitations or high vapor pressure deficit.

TIR data at ECOSTRESS nadir viewing angles exceeding 20° were found to be more susceptible to spatial resolution degradation and misregistration with SR inputs. Limiting to view angles <20° helped to screen retrievals with obvious spatial artifacts such as in Fig. 8. In addition, a number of ECOSTRESS scenes are impacted near the swath edge by solar array intrusion (the ISS moves solar panels to maximize sun angle). These intrusions cannot be automatically flagged, so limiting use to angles <20° is good practice. The reasonable results from ECOSTRESS at lower view angles suggests that the Landsat swath could be effectively doubled (to 14^{O} off nadir) without significant detriment to ET retrieval. The full ECOSTRESS swath could be potentially be used at a lower effective spatial resolution.

The lack of contemporaneous and co-located VSWIR observations reduced the practical utility of ECOSTRESS for ET retrievals using the TSEB-based algorithms employed here, which rely on consistent information about vegetation cover fraction to partition surface temperature between soil and canopy components of the model pixel. Separations of 5 days or larger resulted in 2.5-fold increase in MAE over the ECOSTRESS scenes evaluated here, particularly for cover types with rapid phenological changes such as alfalfa. Work is in progress to migrate from Landsat-only generation of VSWIR inputs (8-day revisit, longer accounting for cloud cover) to use of Harmonized Landsat-Sentinel (HLS) reflectance (3–4 day) fused with MODIS or VIIRS SR to approximate daily filled VSWIR inputs. Cubesat reflectances collected at near daily intervals and cross-calibrated with a standard like Landsat or Sentinel-2 (Houborg and McCabe, 2018; Aragon et al., 2018) have the potential to further improve fidelity in VSWIR inputs on ECOSTRESS overpass dates.

5.2. Value of near-simultaneous TIR/VSWIR acquisition

While multi-source SR fusion has the potential to improve VSWIR inputs to ET retrievals from ECOSTRESS or other TIR free-flying systems, this approach still provides only an approximation of local conditions at the 30-m pixel scale at the time of the thermal sensor overpass. In planning for future thermal missions, several advantages to simultaneous or near-simultaneous TIR/VSWIR acquisition should be considered.

As argued above, simultaneous acquisition ensures that the same surface conditions are being observed in both TIR/VSWIR wavelength regions. This provides for a consistency in information content between TIR and VSWIR that has made Landsat the gold standard in monitoring of land/water-surface phenomena that have a detectable thermal signal. Inconsistencies in land-surface temperature, surface albedo, and vegetation cover inputs due to rapid changes in surface conditions between TIR and VSWIR acquisitions occurring over intervals of a few days (e.g., due to precipitation, irrigation, rapid stress onset, green-up, senescence, harvest, fire or insect damage, or other change agents) can significantly impact the ET retrievals from surface energy balance models, as demonstrated in the case of alfalfa cutting in Fig. 12. The resulting uncertainties may limit or preclude certain TIR applications from a free-flying platform, such as precision irrigation management. Simultaneous acquisition of a modicum of VSWIR bands required to reasonably constrain albedo and LAI minimizes the chance of input inconsistencies.

Second, simultaneous acquisition maximizes scene coverage in applications requiring both TIR and VSWIR inputs. The output coverage is determined by the union of cloud cover at the TIR and VSWIR acquisition times and can only decrease with separation. If part of a scene is missing in either TIR or VSWIR, the temporal mismatch between TIR/VSWIR inputs will be compounded beyond the nominal overpass separation. This is of significant concern for operational monitoring applications in regions of moderate to persistent cloud cover.

Third, simultaneous acquisition facilitates more precise inter-band registration. Misregistration between TIR and VSWIR inputs to ET modeling systems, for example, can result in large retrieval errors in regions of strong heterogeneity in vegetation cover, sharp temperature gradients, or surface moisture status. Attempts to accommodate such

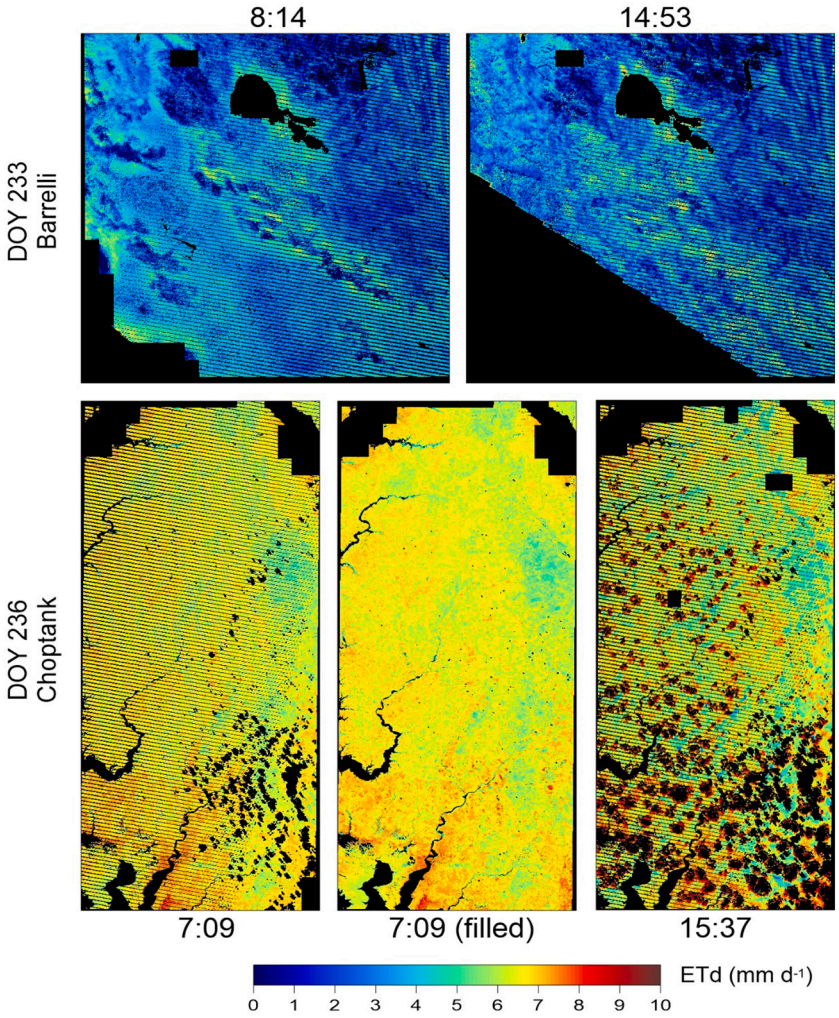

Fig. 11. Impacts of ECOSTRESS overpass time of day on cloud cover in ETd retrievals using (top) LST acquired at 8:14 and 14:43 LT on DOY 233 over Barrelli domain; (bottom) LST acquired at 7:09 (gap-filled ETd map also shown) and 15:37 LT. Stripe gaps are due to scan-line corrector failure on L7 imagery used for VSWIR inputs.

errors result in sacrificing spatial resolution in the thermal inputs (Xue et al., 2020). Landsat's delivery of multi-band (visible, SWIR and TIR) analysis-ready data with precise band-to-band registration has been critical for developing rapid automated processing in support of large area operational applications (Wulder et al., 2019).

TIR/VSWIR separation also impacts the performance of TIR sharpening, which relies on rigorous consistency between thermal and reflective bands. Time separation introduces inconsistency due to changes in surface conditions, differences in topographic shadowing and view angle, unflagged clouds and cloud shadows, and larger errors in co-registration (Xue et al., 2020).

Additionally, TIR/VSWIR consistency is critical for accurate partitioning of ET into soil evaporation (E) and plant transpiration (T). This is particularly crucial for agriculture where transpiration is strongly correlated to biomass accumulation and yield and more accurately informs the grower of actual crop stress (Kool et al., 2014). Soil evaporation and plant transpiration are also key boundary conditions for vadose zone models which are used to simulate solute transport, assess water use/irrigation efficiency and determine crop growth and development (Anderson et al., 2017). Moreover, partitioning into E and T was recently identified a major knowledge gap in ET research (Fisher et al., 2017).

Finally, simultaneous TIR/VSWIR acquisition facilitates cloud detection due to the unique information content provided by these two spectral regions. For example, TIR-only cloud detection with static thresholds will have high commission errors for clouds over frozen surfaces and low-level warm clouds, while VSWIR-only cloud detection will have high commission errors over high reflection targets such as deserts and urban environments – thereby limiting research studies and applications in those environments. However, when combined those commission errors are dramatically reduced due to the complementary nature of optical properties in the VSWIR and TIR bands. Assuming a nominal cloud speed of 20 mph (can be as high as 100 mph for high altitude cirrus), a time separation of 30 s between VSWIR and TIR acquisitions would result in approximately 270 m displacement in cloud/cloud shadows (~10 Landsat pixels). Complete cloud-clearing is critical to many operational applications where extensive manual editing of ET products is prohibitive, particularly those operating at daily to weekly timesteps over large areas. As such, cloud-clearing may be one of the strongest arguments for co-collection as this cannot be addressed through multi-source SR fusion.

6. Conclusion

In this study we assessed the utility of ECOSTRESS LST products from 2018 in mapping ET at sub-field scales with the DisALEXI surface energy balance algorithm, using Landsat ETd retrievals as a baseline for performance. Specifically, impacts on daily ET estimation related to

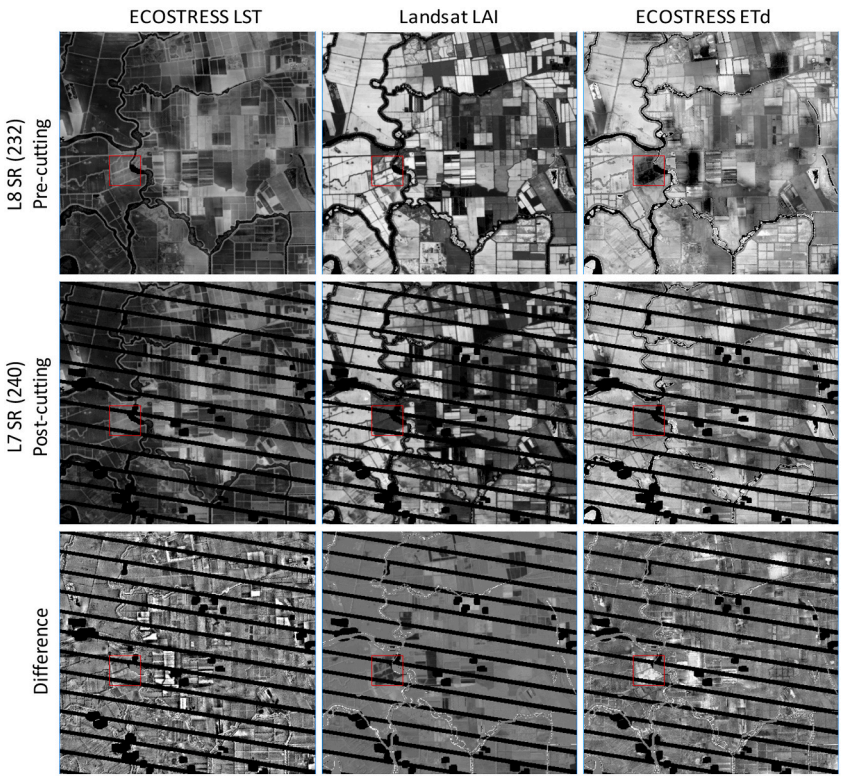

Fig. 12. Impacts on DisALEXI ET retrievals for DOY 239 in using non-coincident VSWIR-TIR inputs over alfalfa fields in Bouldin Island domain. Top row shows sharpened LST, LAI and ETd using SR from DOY 232 (pre-cutting of alfalfa fields highlighted in red box); middle row shows same using SR from DOY 240 (post-cutting); bottom row shows difference maps. (For interpretation of the references to colour in this figure legend, the reader is referred to the web version of this article.)

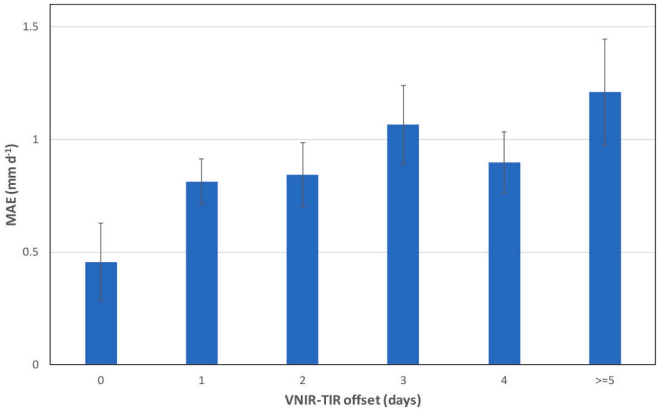

Fig. 13. Average MAE between observed and measured ETd (mm d^{-1}) on ECOSTRESS overpass days for all flux sites combined, binned by offset in days between TIR and VSWIR acquisitions used as input to the SEB model. Error bars represent the standard error in the determination of MAE values within each bin.

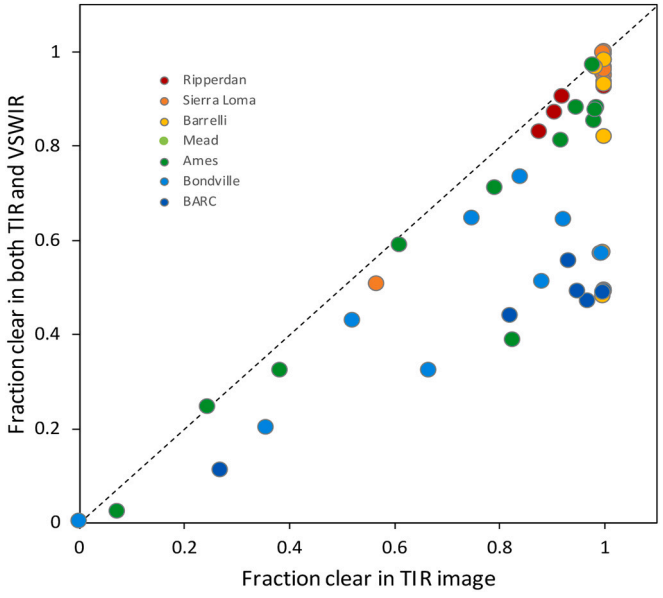

Fig. 14. Reduction in scene coverage due to temporal offset between acquisition of TIR and VSWIR data used as model inputs.

ECOSTRESS temporal sampling frequency, view angle, overpass time, and time separation between TIR and VSWIR data acquisitions were examined both quantitatively and qualitatively.

Comparisons with measurements of ETd from 12 eddy covariance sampling croplands in the United States (CA, NE, IL and MD) showed small improvements in daily ET estimation were achieved on average by including ECOSTRESS retrievals over a Landsat-only scenario. However, significant improvement was observed at individual sites where clear-sky Landsat images were not available during periods of rapid moisture change and vegetation development. In the case of one flux site in MD, mean absolute errors in ET improved by 65% at the daily timestep when critical ECOSTRESS retrievals during the peak soybean crop growth stage were included.

ECOSTRESS LST products were visually found to be at somewhat lower resolution than Landsat 8 TIR images at nadir view angles, and resolution further reduced with increasing view angles. While a SR-based thermal sharpening technique can be used to normalize effective resolution between medium-resolution thermal sensors, ECOSTRESS LST acquisitions at view angles exceeding 20° often yielded poor sharpening results and anomalous ETd retrievals. Still, the augmentation of view angles up to 20° proved to be a benefit in terms of improved temporal sampling in comparison with the Landsat ±7° swath. The disaggregation approach used in DisALEXI accommodated use of ECOSTRESS LST acquired over much of the daylight hours (9:00 a.m. to

5:00 p.m.). While early morning ECOSTRESS LST acquisitions (before 9:00 a.m.) often led to ET maps that were excessively uniform, if paired with a same-day afternoon LST acquisition time-differencing approaches could be implemented. Dependence of cloud cover fraction on acquisition time varied geographically, with some advantage to pre-noon acquisitions at sites in the eastern United States. This conclusion should be revisited using a more extensive archive of ECOSTRESS imagery.

The absence of VSWIR sensors collocated with the TIR bands on ECOSTRESS creates challenges in applications of physically based surface energy balance models that require albedo and LAI or fraction vegetation information consistent with the LST inputs. In this study, VSWIR inputs were obtained from the closest Landsat overpass, and cases where inconsistencies impacted ET retrievals are noted, particularly in landcovers with rapidly changing biomass or moisture limitations. Ongoing work utilizing the Harmonized Landsat-Sentinel dataset for VSWIR inputs will reduce, but not eliminate, the occurrence of significant discrepancy. A major challenge for future possible thermal free-flying sensor architectures will be the development of a rigorous cloud-detection algorithm based only on TIR band information. These efforts include developing a more robust statistical approach to TIR only cloud detection, as opposed to traditional thresholding approaches. Inclusion of one or more collocated SWIR bands (e.g. at 1.38 for cirrus and 1.6 μm for cloud/snow) would enhance cloud detection capabilities as well as geolocation accuracy with VSWIR characterizations of the land-surface.

Declaration of Competing Interest

The authors declare that they have no known competing financial interests or personal relationships that could have appeared to influence the work reported in this paper.

Acknowledgement

The authors wish to thank Dr. Andy Suyker for providing flux data for the Mead field sites. This work was funded in part by the NASA Land Cover Land Use Change Program (NNH14AX36I) and the NASA ECOSTRESS Earth Ventures Instrument project. This research was a contribution from the Long-Term Agroecosystem Research (LTAR) network. LTAR is supported by the United States Department of Agriculture. Part of the research described in this paper was carried out at the Jet Propulsion Laboratory, California Institute of Technology, under contract with the National Aeronautics and Space Administration. © 2020 California Institute of Technology. Government sponsorship acknowledged.

References

Alfieri, J.G., Anderson, M.C., Kustas, W.P., Cammalleri, C., 2017a. Effect of the revisit interval on the accuracy of remote sensing-based estimates of evapotranspiration at field scales. Hydrol. Earth Syst. Sci. 21, 83–98.

Alfieri, J.G., Prueger, J.H., Gish, T.J., Kustas, W.P., McKee, L.G., Russ, A.L., 2017b. The effective evaluation height for flux-gradient relationships and its application to herbicide fluxes. Agric. For. Meteorol. 232, 682–688.

Alfieri, J.G., Kustas, W.P., Prueger, J.H., McKee, L.G., Hipps, L.E., Gao, F., 2019. A multi-year intercomparison of micrometeorological observations at adjacent vineyards in California's Central Valley during GRAPEX. Irrig. Sci. 37, 345–357.

Allen, R.G., Tasumi, M., Morse, A., Trezza, R., Wright, J.L., Bastiaanssen, W.G.M., Kramber, W.J., Lorite, I., Robison, C.W., 2007. Satellite-based energy balance for mapping evapotranspiration with internalized calibration (METRIC) - applications. ASCE J. Irrig. Drainage Eng. 133, 395–406.

Allen, R.G., Pereira, L.S., Howell, T.A., Jensen, M.E., 2011. Evapotranspiration information reporting: I. factors governing measurement accuracy. Agric. Water Manag. 98, 899–920.

Anderson, M.C., 2018. Level-3 Evapotranspiration (ET_ALEXI) Algorithm Theoretical Basis Document. JPL D-94646. https://lpdaac.usgs.gov/documents/332/ECO3ETALEXIU_ATBD_V1.pdf.

Anderson, M.C., Norman, J.M., Diak, G.R., Kustas, W.P., Mecikalski, J.R., 1997. A two-source time-integrated model for estimating surface fluxes using thermal infrared remote sensing. Remote Sens. Environ. 60, 195–216.

Anderson, M.C., Kustas, W.P., Norman, J.M., 2003. Upscaling and downscaling - a regional view of the soil-plant-atmosphere continuum. Agron. J. 95, 1408–1423.

Anderson, M.C., Norman, J.M., Mecikalski, J.R., Torn, R.D., Kustas, W.P., Basara, J.B., 2004. A multi-scale remote sensing model for disaggregating regional fluxes to micrometeorological scales. J. Hydrometeorol. 5, 343–363.

Anderson, M.C., Norman, J.M., Mecikalski, J.R., Otkin, J.A., Kustas, W.P., 2007. A climatological study of evapotranspiration and moisture stress across the continental U.S. based on thermal remote sensing: I. Model formulation. J. Geophys. Res. 112, D10117. https://doi.org/10.1029/2006JD007506.

Anderson, M.C., Allen, R.G., Morse, A., Kustas, W.P., 2012a. Use of Landsat thermal imagery in monitoring evapotranspiration and managing water resources. Remote Sens. Environ. 122, 50–65.

Anderson, M.C., Kustas, W.P., Alfieri, J.G., Hain, C.R., Prueger, J.H., Evett, S.R., Colaizzi, P.D., Howell, T.A., Chavez, J.L., 2012b. Mapping daily evapotranspiration at Landsat spatial scales during the BEAREX'08 field campaign. Adv. Water Resour. 50, 162–177.

Anderson, R.G., Zhang, X., Skaggs, T.H., 2017. Measurement and partitioning of evapotranspiration for application to vadose zone studies. Vadose Zone J. 16.

Anderson, M.C., Gao, F., Knipper, K., Hain, C., Dulaney, W., Baldocchi, D.D., Eichelmann, E., Hemes, K.S., Yang, Y., Medellín-Azuara, J., Kustas, W.P., 2018. Field-scale assessment of land and water use change over the California Delta using remote sensing. Remote Sens. 10, 889.

Anderson, M.C., Diak, G.R., Gao, F., Knipper, K., Hain, C.R., Eichelmann, E., Hemes, K.S., Baldocchi, D.D., Kustas, W.P., Yang, Y., 2019. Impact of insolation data source on remote sensing retrievals of evapotranspiration over the California Delta. Remote Sens. 11, 216.

Aragon, B., Houborg, R., Tu, K., Fisher, J.B., McCabe, M., 2018. Cubesats enable high spatiotemporal retrievals of crop-water use for precision agriculture. Remote Sens. 10, 1867.

Berk, A., Bernstein, L.S., Anderson, G.P., Acharya, P.K., Robertson, D.C., Chetwynd, J.H., Adler-Golden, S.M., 1998. MODTRAN cloud and multiple scattering upgrades with application toAVIRIS. Remote Sens. Environ. 65, 367–375.

Cammalleri, C., Anderson, M.C., Gao, F.H., C.R., & Kustas, W.P., 2014a. Mapping daily evapotranspiration at field scales over rainfed and irrigated agricultural areas using remote sensing data fusion. Agric. For. Meteorol. 186, 1–11.

Cammalleri, C., Anderson, M.C., Kustas, W.P., 2014b. Upscaling of evapotranspiration fluxes from instantaneous to daytime scales for thermal remote sensing applications. Hydrol. Earth Syst. Sci. 18, 1885–1894.

Cook, M., Mandel, J., Raqueno, N., Schott, J.R., 2014. Development of an operational calibration methodology for the Landsat thermal data archive and initial testing of the atmospheric compensation component of a land surface temperature (LST) product from the archive. Remote Sens. 6, 11244–11266.

Cuenca, R.H., Ciotti, S.P., Hagimoto, Y., 2013. Application of landsat to evaluate effects of irrigation forbearance. Remote Sens. 5, 3776–3802.

Eichelmann, E., Hemes, K.S., Knox, S.H., Oikawa, P., Chamberlain, S.D., Sturtevant, C., Verfaillie, J., Baldocchi, D.D., 2018. The effect of land cover type and structure on evapotranspiration from agricultural and wetland sites in the Sacramento/San Joaquin River Delta, California. Agric. For. Meteorol. 256-257, 179–195.

Fisher, J.B., Tu, K., Baldocchi, D.D., 2008. Global estimates of the land-atmosphere water flux based on monthly AVHRR and ISLSCP-II data, validated at 16 FLUXNET sites. Remote Sens. Environ. 112, 901–919.

Fisher, J.B., Melton, F.S., Middleton, E.M., Hain, C.R., Anderson, M.C., Allen, R.G., McCabe, M.F., Hook, S., Baldocchi, D.D., Townsend, P.A., Kilic, A., Tu, K., Miralles, D.D., Perret, J., Lagouarde, J.-P., Waliser, D., Purdy, A.J., French, A.N., Schimel, D., Famiglietti, J.S., Stephens, G., Wood, E.F., 2017. The future of evapotranspiration: global requirements for ecosystem functioning, carbon and climate feedbacks, agricultural management, and water resources. Water Resour. Res. 53, 2618–2626.

Fisher, J.B., Lee, B., Purdy, A.J., Halverson, G.H., Dohlen, M.B., Cawse-Nicholson, K., Wang, A., Anderson, R.G., Aragon, B., Arain, M.A., Baldocchi, D.D., Baker, J.M., Barral, H., Bernacchi, C.J., Bernhofer, C., Biraud, S.C., Bohrer, G., Brunsell, N., Cappelaere, B., Castro-Contreras, S., Chun, J., Conrad, B.J., Cremonese, E., Demarty, J., Desai, A.R., De Ligne, A., Foltýnová, L., Goulden, M.L., Griffis, T.J., Grünwald, T., Johnson, M.S., Kang, M., Kelbe, D., Kowalska, N., Lim, J.H., Maïnassara, I., McCabe, M.F., Missik, J.E.C., Mohanty, B.P., Moore, C.E., Morillas, L., Morrison, R., Munger, J.W., Posse, G., Richardson, A.D., Russell, E.S., Ryu, Y., Sanchez-Azofeifa, A., Schmidt, M., Schwartz, E., Sharp, I., Šigut, L., Tang, Y., Hulley, G., Anderson, M., Hain, C., French, A., Wood, E., Hook, S., 2020. ECOSTRESS: NASA's next generation Mission to measure evapotranspiration from the international Space Station. Water Resour. Res. 56 e2019WR026058.

Gao, F., Masek, J., Schwaller, M., Hall, F.G., 2006. On the blending of the Landsat and MODIS surface reflectance: predicting daily Landsat surface reflectance. IEEE Trans. Geosci. Remote Sens. 44, 2207–2218.

Gao, F., Anderson, M.C., Kustas, W.P., Wang, Y., 2012a. A simple method for retrieving leaf area index from Landsat using MODIS LAI products as reference. J. Appl. Remote. Sens. 6 https://doi.org/10.1117/.JRS.1116.063554.

Gao, F., Kustas, W.P., Anderson, M.C., 2012b. A data mining approach for sharpening thermal satellite imagery over land. Remote Sens. 4, 3287–3319.

Gelaro, R., McCarty, W., Suárez, M.J., Todling, R., Molod, A., Takacs, L., Randles, C.A., Darmenov, A., Bosilovich, M.G., Reichle, R., Wargan, K., Coy, L., Cullather, R., Draper, C., Akella, S., Buchard, V., Conaty, A., da Silva, A.M., Gu, W., Kim, G.K., Koster, R., Lucchesi, R., Merkova, D., Nielsen, J.E., Partyka, G., Pawson, S., Putman, W., Rienecker, M., Schubert, S.D., Sienkiewicz, M., Zhao, B., 2017. The modern-era retrospective analysis for research and applications, version 2 (MERRA-2). J. Clim. 30, 5419–5454.

Gillespie, A., Rokugawa, S., Matsunaga, T., Steven Cothern, J., Hook, S., Kahle, A.B., 1998. A temperature and emissivity separation algorithm for advanced spaceborne

thermal emission and reflection radiometer (ASTER) images. IEEE Trans. Geosci. Remote Sens. 36, 1113–1126.
Gish, T.J., Walthall, C.L., Daughtry, C.S.T., Dulaney, W.P., McCarty, G.W., 2003. Watershed-scale sensing of subsurface flow pathways at OPE3 site. In: First Interagency Conference on Research in the Watersheds, pp. 192–197. Benson, AZ.
Guillevic, P.C., Olioso, A., Hook, S.J., Fisher, J.B., Lagouarde, J.P., Vermote, E.F., 2019. Impact of the revisit of thermal infrared remote sensing observations on evapotranspiration uncertainty-a sensitivity study using AmeriFlux data. Remote Sens. 11, 573.
Guzinski, R., Anderson, M.C., Kustas, W.P., Nieto, H., Sandholt, I., 2013. Using a thermal-based two source energy balance model with time-differencing to estimate surface energy fluxes with day-night MODIS observations. Hydrol. Earth Syst. Sci. 17, 2809–2825.
Hemes, K.S., Chamberlain, S.D., Eichelmann, E., Anthony, T., Valach, A., Kasak, K., Szutu, D., Verfaillie, J., Silver, W.L., Baldocchi, D.D., 2019. Assessing the carbon and climate benefit of restoring degraded agricultural peat soils to managed wetlands. Agric. For. Meteorol. 268, 202–214.
Houborg, R., McCabe, M.F., 2018. Daily retrieval of NDVI and LAI at 3 m resolution via the fusion of CubeSat, Landsat, and MODIS data. Remote Sens. 10, 890.
Houborg, R., Anderson, M.C., Daughtry, C.S.T., Kustas, W.P., Rodell, M., 2011. Using leaf chlorophyll to parameterize light-use-efficiency within a thermal-based carbon, water and energy exchange model. Remote Sens. Environ. 115, 1694–1705.
Hulley, G., Hook, S., 2018a. ECOSTRESS Level-2 Cloud Detection Algorithm Theoretical Basis Document (ATBD). JPL D-94644. https://lpdaac.usgs.gov/documents/296/ECO2_Cloud_ATBD_V1.pdf.
Hulley, G., Hook, S., 2018b. ECOSTRESS Level-2 Land Surface Temperature and Emissivity Algorithm Theoretical Basis Document (ATBD). JPL D-94643. https://lpdaac.usgs.gov/documents/297/ECO2_LSTE_ATBD_V1.pdf.
Kalma, J.D., McVicar, T.R., McCabe, M.F., 2008. Estimating land surface evaporation: a review of methods using remotely sensing surface temperature data. Surv. Geophys. https://doi.org/10.1007/s10712-10008-19037-z.
Karimi, P., Bastiaanssen, W.G.M., Molden, D., 2013. Water accounting plus (WA+) - a water accounting procedure for complex river basins based on satellite measurements. Hydrol. Earth Syst. Sci. 17, 2459–2472.
Kleinman, P.J.A., Spiegal, S., Rigby, J.R., Goslee, S.C., Baker, J.M., Bestelmeyer, B.T., Boughton, R.K., Bryant, R.B., Cavigelli, M.A., Derner, J.D., Duncan, E.W., Goodrich, D.C., Huggins, D.R., King, K.W., Liebig, M.A., Locke, M.A., Mirsky, S.B., Moglen, G.E., Moorman, T.B., Pierson, F.B., Robertson, G.P., Sadler, E.J., Shortle, J. S., Steiner, J.L., Strickland, T.C., Swain, H.M., Tsegaye, T., Williams, M.R., Walthall, C.L., 2018. Advancing the sustainability of US agriculture through long-term research. J. Environ. Qual. 47, 1412–1425.
Knipper, K., Kustas, W.P., Anderson, M.C., Alsina, M., Hain, C., Alfieri, J.G., Prueger, J., Gao, F., McKee, L., Sanchez, L.A., 2019a. Using high-spatiotemporal thermal satellite ET retrievals for operational water use and stress monitoring in a California vineyard. Remote Sens. 11, 2124.
Knipper, K.R., Kustas, W.P., Anderson, M.C., Alfieri, J.G., Prueger, J.H., Hain, C.R., Gao, F., Yang, Y., McKee, L.G., Nieto, H., Hipps, L.E., Alsina, M.M., Sanchez, L., 2019b. Evapotranspiration estimates derived using thermal-based satellite remote sensing and data fusion for irrigation management in California vineyards. Irrig. Sci. 37, 431–449.
Knipper, K.R., Kustas, W.P., Anderson, M.C., Nieto, H., Alfieri, J.G., Prueger, J.H., Hain, C.R., Gao, F., McKee, L.G., Alsina, M., Sanchez, L., 2020. Using high-spatiotemporal thermal satellite ET retrievals to monitor water use over California vineyards of different climate, vine variety and trellis design. Water Resour. Res. 241, 106361.
Kool, D., Agam, N., Lazarovitch, N., Heitman, J.L., Sauer, T.J., Ben-Gal, A., 2014. A review of approaches for evapotranspiration partitioning. Agric. For. Meteorol. 184, 56–70.
Kustas, W.P., Anderson, M.C., 2009. Advances in thermal infrared remote sensing for land surface modeling. Agric. For. Meteorol. 149, 2071–2081.
Kustas, W.P., Norman, J.M., 1999. Evaluation of soil and vegetation heat flux predictions using a simple two-source model with radiometric temperatures for partial canopy cover. Agric. For. Meteorol. 94, 13–29.
Kustas, W.P., Norman, J.M., 2000. A two-source energy balance approach using directional radiometric temperature observations for sparse canopy covered surfaces. Agron. J. 92, 847–854.
Kustas, W.P., Diak, G.R., Norman, J.M., 2001. Time difference methods for monitoring regional scale heat fluxes with remote sensing. Land Surf. Hydrol. Meteorol. Clim.: Observ. Model. 3, 15–29.
Kustas, W.P., Alfieri, J.G., Evett, S., Agam, N., 2015. Quantifying variability in field-scale evapotranspiration measurements in an irrigated agricultural region under advection. Irrig. Sci. 33, 325–338.
Kustas, W.P., Anderson, M.C., Alfieri, J.G., Knipper, K., Torres-Rua, A., Parry, C.K., Nieto, H., Agam, N., White, A., Gao, F., McKee, L., Prueger, J.H., Hipps, L.E., Los, S. O., Alsina, M., Sanchez, L., Sams, B., Dokoozlian, N., McKee, M., Jones, S., McElrone, A., Heitman, J.L., Howard, A.M., Post, K., Melton, F.S., Hain, C., 2018. The grape remote sensing atmospheric profile and evapotranspiration eXperiment (GRAPEX). Bull. Am. Meteorol. Soc. 99, 1791–1812.
Leuning, R., Raupach, M.R., Coppin, P.A., Cleugh, H.A., Isaac, P., Denmead, O.T., Dunin, F.X., Zegelin, S., Hacker, J., 2004. Spatial and temporal variations in fluxes of energy, water vapour and carbon dioxide during OASIS 1994 and 1995. Bound.-Layer Meteorol. 110, 3–38.
Liang, S., 2000. Narrowband to broadband conversions of land surface albedo I algorithms. Remote Sens. Environ. 76, 213–238.
Mauder, M., Genzel, S., Fu, J., Kiese, R., Soltani, M., Steinbrecher, R., Zeeman, M., Banerjee, T., De Roo, F., Kunstmann, H., 2018. Evaluation of energy balance closure adjustment methods by independent evapotranspiration estimates from lysimeters and hydrological simulations. Hydrol. Process. 32, 39–50.
McCarty, G.W., McConnell, L.L., Hapeman, C.J., Sadeghi, A., Graff, C., Hively, W.D., Lang, M.W., Fisher, T.R., Jordan, T., Rice, C.P., Codling, E.E., Whitall, D., Lynn, A., Keppler, J., Fogel, M.L., 2008. Water quality and conservation practice effects in the Choptank River watershed. J. Soil Water Conserv. 63, 461–474.
Mecikalski, J.M., Diak, G.R., Anderson, M.C., Norman, J.M., 1999. Estimating fluxes on continental scales using remotely-sensed data in an atmosphere-land exchange model. J. Appl. Meteorol. 38, 1352–1369.
Medellín-Azuara, J., Paw, U.K.T., Jin, Y., Kent, E., Clay, J., Wong, A., Bell, A., Anderson, M., Howes, D., Melton, F.S., Kadir, T., Orang, M., Leinfelder-Miles, M.M., Lund, J., 2018. A Comparative Study for Estimating Crop Evapotranspiration in the Sacramento-San Joaquin Delta. https://watershed.ucdavis.edu/project/delta-et.
Meyers, T.P., Hollinger, S.E., 2004. An assessment of storage terms in the surface energy balance of maize and soybean. Agric. For. Meteorol. 125, 105–115.
Norman, J.M., Kustas, W.P., Humes, K.S., 1995. A two-source approach for estimating soil and vegetation energy fluxes from observations of directional radiometric surface temperature. Agric. For. Meteorol. 77, 263–293.
Norman, J.M., Kustas, W.P., Prueger, J.H., Diak, G.R., 2000. Surface flux estimation using radiometric temperature: a dual temperature difference method to minimize measurement error. Water Resour. Res. 36, 2263–2274.
Norman, J.M., Anderson, M.C., Kustas, W.P., French, A.N., Mecikalski, J.R., Torn, R.D., Diak, G.R., Schmugge, T.J., Tanner, B.C.W., 2003. Remote sensing of surface energy fluxes at 10^1-m pixel resolutions. Water Resour. Res. 39, 1221.
Prueger, J.H., Hatfield, J.L., Kustas, W.P., Hipps, L.E., MacPherson, J.I., Parkin, T.B., 2005. Tower and aircraft eddy covariance measurements of water vapor, energy and carbon dioxide fluxes during SMACEX. J. Hydrometeorol. 6, 954–960.
Ryu, Y., Baldocchi, D.D., Black, T.A., Detto, M., Law, B.E., Leuning, R., Miyata, A., Reichstein, M., Vargas, R., Amman, C., Beringeri, J., Flanagan, L.B., Gu, L., Hutley, L. B., Kim, J., McCaughey, H., Moors, E.D., Rambal, S., Vesala, T., 2012. On the temporal upscaling of evapotranspiration from instantaneous remote sensing measurements to 8-day mean daily-sums. Agric. For. Meteorol. 152, 212–222.
Saha, S., Moorthi, S., Wu, X., Wang, J., Nadiga, J., Behringer, D., Hou, Y., Chuang, H., Iredell, M., Ek, M., 2014. The NCEP climate forecast system version 2. J. Clim. 27, 2185–2208.
Saunders, R., Hocking, J., Turner, E., Rayer, P., Rundle, D., Brunel, P., Vidot, J., Roquet, P., Matricardi, M., Geer, A., Bormann, N., Lupu, C., 2018. An update on the RTTOV fast radiative transfer model (currently at version 12). Geosci. Model Dev. 11, 2717–2737.
Semmens, K.A., Anderson, M.C., Kustas, W.P., Gao, F., Alfieri, J.G., McKee, L., Prueger, J. H., Hain, C.R., Cammalleri, C., Yang, Y., Xia, T., Vélez, M., Sanchez, L., Alsina, M., 2015. Monitoring daily evapotranspiration over two California vineyards using Landsat 8 in a multi-sensor data fusion approach. Remote Sens. Environ. https://doi.org/10.1016/j.rse.2015.1010.1025.
Senay, G.B., Friedrichs, M., Singh, R.K., Velpuri, N.M., 2016. Evaluating Landsat 8 evapotranspiration for water use mapping in the Colorado River Basin. Remote Sens. Environ. 185, 171–185.
Sun, L., Anderson, M.C., Gao, F., Hain, C.R., Alfieri, J.G., Sharifi, A., McCarty, G., Yang, Y., Yang, Y., 2017. Investigating water use over the Choptank River watershed using a multi-satellite data fusion approach. Water Resour. Res. 53, 5298–5319.
Suyker, A.E., Verma, S.B., Burba, G.G., Arkebauer, T.J., Walters, D.T., Hubbard, K.G., 2004. Growing season carbon dioxide exchange in irrigated and rainfed maize. Agric. For. Meteorol. 124, 1–13.
Tuzet, A., Perrier, A., Leuning, R., 2003. A coupled model of stomatal conductance, photosynthesis and transpiration. Plant Cell Environ. 26, 1097–1116.
Twine, T.E., Kustas, W.P., Norman, J.M., Cook, D.R., Houser, P.R., Meyers, T.P., Prueger, J.H., Starks, P.J., Wesely, M.L., 2000. Correcting eddy-covariance flux underestimates over a grassland. Agric. For. Meteorol. 103, 279–300.
Whitcraft, A.K., Becker-Reshef, I., Justice, C.O., 2015. A framework for defining spatially explicit earth observation requirements for a global agricultural monitoring initiative (GEOGLAM). Remote Sens. 7, 1461–1481.
Wu, Z., Snyder, G., Vadnais, C., Arora, R., Babcock, M., Stensaas, G., Doucette, P., Newman, T., 2019. User needs for future Landsat missions. Remote Sens. Environ. 231, 111214.
Wulder, M.A., Loveland, T.R., Roy, D.P., Crawford, C.J., Masek, J.G., Woodcock, C.E., Allen, R.G., Anderson, M.C., Belward, A.S., Cohen, W.B., Dwyer, J., Erb, A., Gao, F., Griffiths, P., Helder, D., Hermosilla, T., Hipple, J.D., Hostert, P., Hughes, M.J., Huntington, J., Johnson, D.M., Kennedy, R., Kilic, A., Li, Z., Lymburner, L., McCorkel, J., Pahlevan, N., Scambos, T.A., Schaaf, C., Schott, J.R., Sheng, Y., Storey, J., Vermote, E., Vogelmann, J., White, J.C., Wynne, R.H., Zhu, Z., 2019. Current status of Landsat program, science, and applications. Remote Sens. Environ. 225, 127–147.
Xue, J., Anderson, M.C., Gao, F., Hain, C., Sun, L., Yang, Y., Knipper, K.R., Kustas, W.P., Torres-Rua, A., Schull, M.A., 2020. Sharpening ECOSTRESS and VIIRS land surface temperature using harmonized Landsat-sentinel surface reflectance. Remote Sens. Environ. 251, 112055.
Yang, Y., Anderson, M.C., Gao, F., Hain, C.R., Semmens, K.A., Kustas, W.P., Normeets, A., Wynne, R.H., Thomas, V.A., Sun, G., 2017. Daily Landsat-scale evapotranspiration estimation over a managed pine plantation in North Carolina, USA using multi-satellite data fusion. Hydrol. Earth Syst. Sci. 21, 1017–1037.
Yang, Y., Anderson, M.C., Gao, F., Wardlow, B., Hain, C.R., Otkin, J.A., Alfieri, J., Yang, Y., Sun, L., Dulaney, W., 2018. Field-scale mapping of evaporative stress indicators of crop yield: an application over Mead, NE, USA. Remote Sens. Environ. 210, 387–402.
Yang, Y., Anderson, M., Gao, F., Hain, C., Noormets, A., Sun, G., Wynne, R., Thomas, V., Sun, L., 2020. Investigating impacts of drought and disturbance on

evapotranspiration over a forested landscape in North Carolina, USA using high spatiotemporal resolution remotely sensed data. Remote Sens. Environ. 238, 111018.